DESIGN AND CONSTRUCTION OF A TWIN RUBY LASER

By

LARRY JOE PEERY

Bachelor of Science

Missouri University at Rolla

Rolla, Missouri

1964

Submitted to the Faculty of the Graduate College
of the Oklahoma State University
in partial fulfillment of the requirements
for the degree of
MASTER OF SCIENCE
July, 1967

VITA

Larry Joe Peery

Candidate for the Degree of

Master of Science

Thesis: DESIGN AND CONSTRUCTION OF A TWIN RUBY LASER

Major Field: Physics

Biographical:

Personal Data: Born in Moberly, Missousi, December 24, 1941, the son of James M. and Minnie L. Peery

Education: Attended grade school in Moberly, Missouri; graduated from St. Charles High School, St. Charles, Missouri in 1959; received the Bachelor of Science degree from the Missouri University at Rolla, with a major in Physics, in May, 1964; completed requirements for the Master of Science degree in July, 1967.

Professional Experience: Co-operative Training Student with McDonnell Douglas Corporation of St. Louis during pursuit of undergraduate studies; Teaching Assistant in Physics Department, Oklahoma State University; Research Assistant for the Oklahoma State University Research Foundation; Member of Sigma Pi Sigma; Ensign in Research Reserve, United States Navy.

DESIGN AND CONSTRUCTION OF A

TWIN RUBY LASER

Thesis Approved:

Francis C. Todd

Thesis Adviser

K. Harrington

Leon W. Schmeder

Dean of the Graduate College

PREFACE

This work was undertaken at the suggestion of Dr. F. C. Todd who acted as the author's adviser and project supervisor. The purpose of this research was to design and construct a laser facility to be used in plasma studies.

This facility is to be used in various plasma studies, in an attempt to understand the physical processes which occur upon laser beam impact on metallic surfaces. The principle target material of interest will be aluminum.

The assistance and guidance of Dr. Todd have been invaluable in the completion of this work. The author is also grateful to Mr. W. G. Robinson and H. G. Gurney for their assistance in the construction of the laser facility.

The work was carried out under NASA Contract Number NASr-7 administered through the Research Foundation, Oklahoma State University.

TABLE OF CONTENTS

LIST OF FIGURES

LIST OF FIGURES (CONTINUED)

CHAPTER I

INTRODUCTION

The phenomena associated with laser beam impact on metallic surfaces has evoked considerable interest as is demonstrated by the current literature (Gregg, 1966; Vogel, 1965). It has been found that the target deformation is of two general types, dependent on the rate at which radiant energy is supplied to the surface under study. The one type of deformation, which occurs at relatively low rates of energy input, consists of a deep hole which is approximately the same diameter as the laser beam at the surface and tapers to a point. The other deformation is characterized by a crater shape and is relatively shallow.

These two types of target deformation are suggestive of the deformations found in particle impacts. The first type of deformation occurs in low velocity particle impacts, and the second is observed in hypervelocity particle impacts. Another similarity between hypervelocity particle impact and the laser beam impact at high power levels, is the appearance of a plasma at the region of impact. Because of the similarities between the two processes, a study of laser beam impact involving high rates of energy input to the target has been undertaken.

In order to undertake an experimental study of laser beam impact, it was necessary to design and construct a laser system with a high power level. For this reason, a q-switched, two ruby laser system was chosen. In addition, an output with a well-defined energy variation

with time was desired. To achieve this, the system was designed to be operated in a q-switched mode. Without the q-switch, it may also be operated in the conventional mode. In order to obtain the most uniform distribution of energy across the section of the laser beam, helical flashtubes were selected to excite the two rubies. It was well-known that this excitation would be less efficient than straight flashtubes but efficiency was sacrificed for a more uniform intensity. The two helical flashtubes are powered by twin, capacitor banks which are rated at 27 kilojoules each and which are operated at 10,000 volts.

The laser facility was designed to be employed in conjunction with an ultraviolet spectrograph which was available in the laboratory. This spectrograph was designed to study the radiation from the plasma which occurs in particle impact. In addition, a quadrupole mass spectrometer is planned which will yield data concerning the number density, as a function of time, of various species of ions in the plasma.

This thesis describes the design and construction of the laser facility. In addition, the working equations for the quadrupole mass spectrometer are presented. The results of initial tests on the laser facility in the conventional mode are also included in a qualitative fashion. In conclusion, various suggestions as to future improvements of the facility are presented.

CHAPTER II

THEORETICAL DISCUSSION

The term laser is formed from the words "Light Amplification by Stimulated Emission of Radiation", and it is applied to various devices which are capable of this process. Most of these devices are employed as a generator of radiation by providing feedback to initiate an amplified pulse of light. In this section, the basic theory of lasers (Lengyel, 1966) will be presented with an explanation of the conditions for laser activity. In the last section of this chapter, a qualitative description is presented of the more complex theory which deals with the particular type of ruby laser that was developed for our laboratory.

General Theory

To achieve light amplification in a given medium, the medium must be placed in a state of negative absorption. This state of negative absorption is produced by creating a population inversion between the atomic energy levels of the system. The physical conditions necessary for the attainment of a population inversion in a three level, atomic system are considered in this section. The ruby laser, which is basically a three level system, is described as a practical example of the conditions for light amplification.

The term "population inversion" may be explained by reference to Figure 2.1 where a simplified energy level diagram is shown.

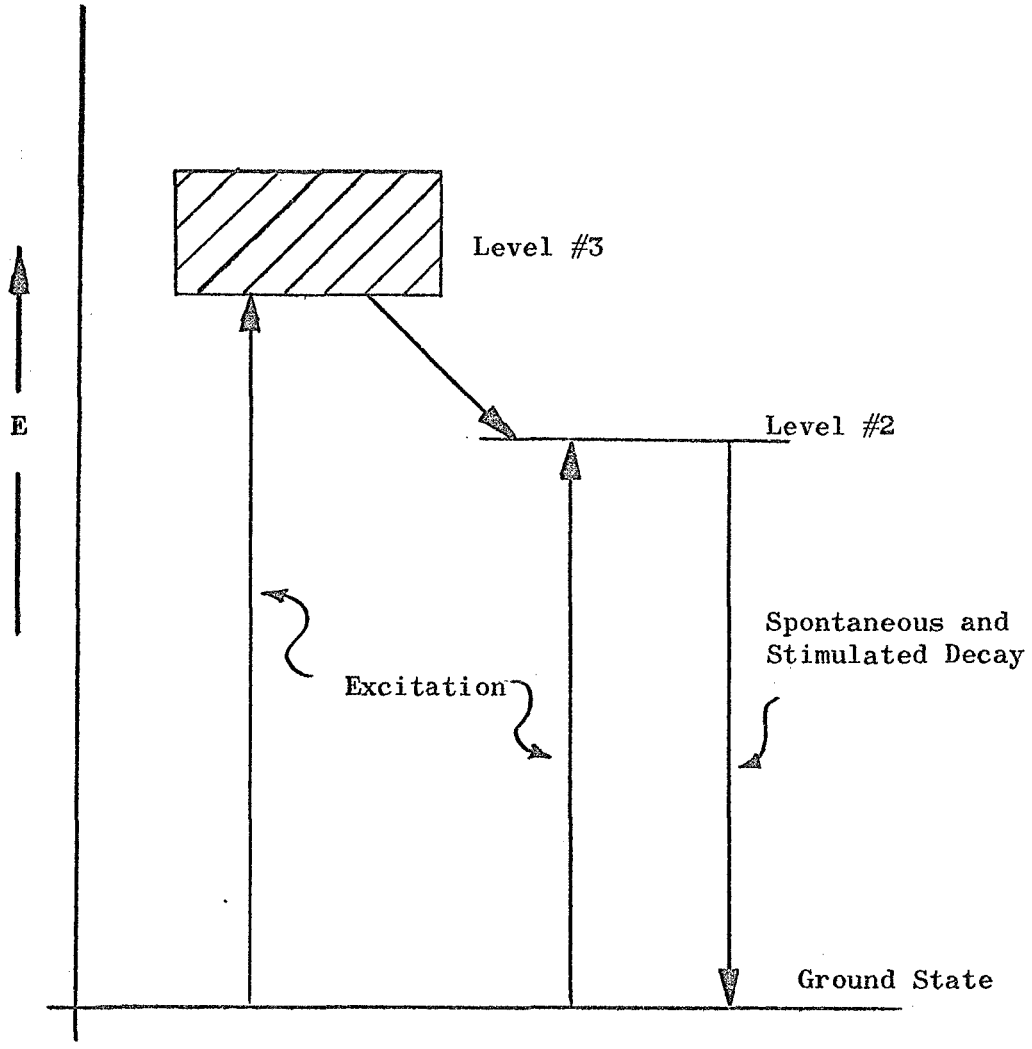

Figure 2.1. Simplified Energy Level Diagram.

When excitation is applied to the laser medium, its absorption causes transitions from the ground state to the broad-band energy level #3. The decay of this excited state at low intensities is a two step process. One step consists of a radiationless (phonon emission) decay to the sharp level, #2. The second step is a relatively slow decay to the ground state. This decay to the ground state results in spontaneous light emission, and is responsible for the phenomena of fluorescence which is observed for all levels of excitation. If sufficient radiation is absorbed during the excitation, the number of atoms of the laser material in state #2 will be greater than the number in state #1. This phenomena is known as population inversion, and leads to light amplification. The light emitted within the medium as a result of fluorescence, will stimulate additional transitions from level #2 to the ground state. This additional radiation is termed stimulated emission, and is responsible for the laser output.

In order to describe the above process quantitatively, consider the atomic processes of absorption and emission. A large number of atoms in thermal equilibrium at a temperature, T, will obey the Boltzmann distribution; that is

$$N_j' = \frac{N_o\, e^{-E_j/kT}}{\sum_i e^{-E_i/kT}} \qquad (2.1)$$

where, N_j' = population of j^{th} state

E_j = energy of j^{th} state.

If there are g_n states/energy level, then these will be equally occupied, and

$$N_n' = \frac{N_n}{g_n} \tag{2.2}$$

where, N_n = population of the n^{th} energy level.

Thus, the ratio of populations for the n^{th} and m^{th} level will be given by

$$\frac{N_n}{N_m} = \frac{g_n}{g_m} \; e^{-(E_n - E_m)/kT} \tag{2.3}$$

where E_n and E_m are measured from the ground state at zero temperature. At thermal equilibrium, the lower states are more densely populated than the higher states. However, as radiation is absorbed, this equilibrium is disturbed.

Assume a parallel beam of light with a frequency between ν and $\nu + d\nu$ and with an intensity, I_ν, which is traveling in the positive x direction through a layer of atoms that are bounded by x and x + dx. If N_1 atoms/cm^3 are in level #1, of which $dN_{1\nu}$ absorb light of a frequency between ν and $\nu + d\nu$, and $dN_{2\nu}$ atoms/cm^3 emit in this spectral band, then the decrease in intensity is

$$-d(I_\nu d\nu) = h\nu(B_{12}dN_{1\nu} - B_{21}dN_{2\nu})\, I_\nu dt \tag{2.4}$$

where, B_{21} = Einstein coefficient for stimulated emission

B_{12} = Einstein coefficient for stimulated absorption

The definition for the velocity of light in a medium is

$$dt = \frac{dx}{V} = \frac{dx\eta}{c}$$

where, v = velocity of light in the medium

= c/η

with c, the velocity of light in vacuum, and η the index of refraction for the material. Substitute in (2.4)

$$-d(I_\nu d\nu) = \frac{h\nu\eta}{c} (B_{12}dN_{1\nu} - B_{21}dN_{2\nu})I_\nu dx \qquad (2.5)$$

or,

$$-\frac{1}{I_\nu} \frac{dI_\nu}{dx} d\nu = \frac{h\nu\eta}{c} (B_{12}dN_{1\nu} - B_{21}dN_{2\nu}) \qquad (2.6)$$

The absorption coefficient of a medium, k_ν, is given by the relation,

$$I_\nu(x) = I_o e^{-k_\nu x} \qquad (2.7)$$

hence,

$$\frac{dI_\nu}{dx} = -k_\nu I_\nu \qquad (2.8)$$

or,

$$-\frac{1}{I_\nu} \frac{dI_\nu}{dx} d\nu = k_\nu d\nu \qquad (2.9)$$

By substitution, Equation (2.6) becomes,

$$k_\nu d\nu = \frac{h\nu\eta}{c} (B_{12}dN_{1\nu} - B_{21}dN_{2\nu}) \qquad (2.10)$$

By integrating the absorption, k_ν, over the absorption line centered about ν_o, one obtains

$$\int k_\nu d\nu = \frac{h\nu_o\eta}{c} (B_{12}N_1 - B_{21}N_2) \qquad (2.11)$$

where it has been assumed that the frequency does not vary appreciably from ν_o over the absorbtion line. The Einstein coefficient for spontaneous emission A_{nm} is related to the stimulated transition coefficient by

$$g_n B_{nm} = g_m B_{mn} \qquad (2.12)$$

and,

$$B_{nm} = \frac{c^3}{8\pi h\nu^3\eta^3} A_{nm}$$

Then Equation (2.11) becomes

$$\int k_\nu d_\nu = \frac{c^2 A_{21}}{8\pi\nu_o^2\eta^2} (N_1 - \frac{g_1}{g_2} N_2) \qquad (2.13)$$

From Equation (2.13), a condition of amplification exists provided the population of level #2 is sufficiently greater than that of level #1; i.e., a condition of negative absorption exists.

Before proceeding, it is necessary to define and derive several more relations for the absorption coefficient. Represent k_ν by

$$k_\nu = \kappa g(\nu; \nu_o) \tag{2.14}$$

where, $g(\nu; \nu_o)$ is the normalized, absorption lineshape; i.e.,

$$\int_0^\infty g(\nu; \nu_o)\, d\nu = 1$$

Then, it is found that

$$\int_0^\infty k_\nu d\nu = \kappa \int_0^\infty g(\nu; \nu_o)\, d\nu = \kappa$$

Thus, the peak absorption, which occurs at a frequency of ν_o is given by,

$$k_m = \left(\int_0^\infty k_\nu d_\nu\right) g(\nu_o; \nu_o) \tag{2.15}$$

For low levels of excitation, Equation (2.13) takes the form,

$$\int_0^\infty k_\nu d_\nu = \kappa N_o \tag{2.16}$$

where, $N_1 = N_o$

with N_o being the total number of atoms present. If it is assumed that the absorption line shape remains the same, i.e., $g(\nu; \nu_o)$ is independent of excitation level, Equations (2.13, 2.14, and 2.15) may be employed to obtain the ratio

$$\frac{k_m}{k_o} = \frac{\kappa\, g(\nu_o; \nu_o)}{\kappa\, g(\nu_o; \nu_o)} = \frac{N_1 - \left(\frac{g_1}{g_2}\right) N_2}{N_o} \tag{2.17}$$

where k_o = peak absorption for low levels of excitation

k_m = peak absorption for high levels of excitation.

If by some means, a material may be placed into a state of negative absorption, a light beam of frequency, ν, will grow exponentially on

passing through the media, according to the relation,

$$I = I_o e^{\alpha x} \tag{2.18}$$

where,

$$\alpha = - k_\nu$$

and laser activity may occur. To determine the conditions under which laser action occurs, consider a possible arrangement such as illustrated in Figure 2.2. The partial reflector is necessary in order to obtain an output from the laser and to sustain operation. As a result of both spontaneous and stimulated emission, light is generated within the laser medium. The light which is not lost through the sides travels through the medium and is reflected back and forth between the reflectors. If the partial reflector has a reflectance of r and is loss-less, an intensity of (1-r) is lost on each reflection at the partial reflector. Oscillations are only sustained provided the energy gain in the laser medium is equal to or greater than the energy losses at the partial reflector. There are secondary losses which occur but these will be neglected in this discussion.

On each pass through the system, shown as the light path 1-2-3-4-5-6,

$$I_6 = I_1 r e^{2\alpha L} \tag{2.19}$$

Define a loss coefficient, γ, as

$$\gamma = - \ell nr \tag{2.20}$$

then

$$I_6 = I_1 e^{2\alpha L - \gamma} \tag{2.21}$$

When the factor $e^{2\alpha L-\gamma}$ is greater than unity, the oscillations within the cavity will increase; and when it is less than one, they decay. The threshold condition is, therefore, given by

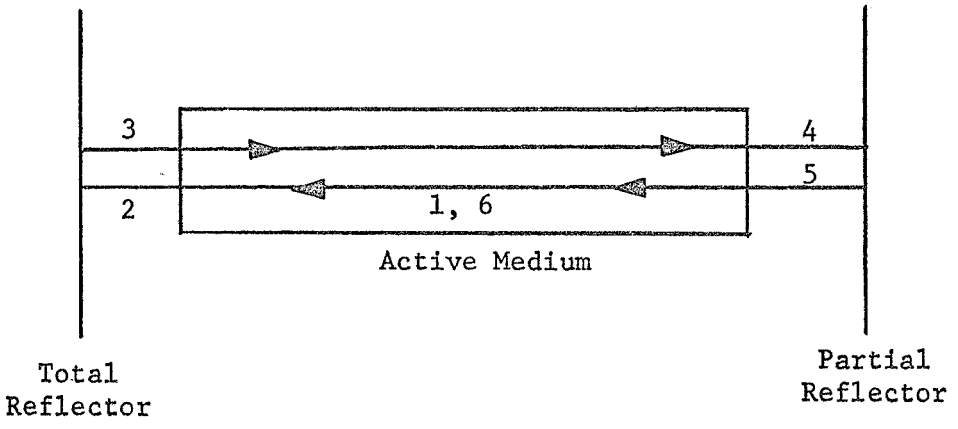

Figure 2.2. Schematic Diagram of Laser.

$$\alpha = \frac{\gamma}{2L} \tag{2.22}$$

In a three level system such as the one that is illustrated in Figure 2.3, the following system of rate equations are valid (Lengyel, 1966).

$$\text{(a)} \quad N_o = N_1 + N_2 + N_3$$

$$\text{(b)} \quad \frac{dN_3}{dt} = W_{13}N_1 - (W_{31} + A_{31} + S_{32})\, N_3 \tag{2.23}$$

$$\text{(c)} \quad \frac{dN_2}{dt} = W_{12}N_1 - (W_{21} + A_{21})\, N_2 + S_{32}N_3$$

The W's are the probabilities of stimulated transitions, which depend on the energy density. The A's are the probabilities of spontaneous transitions, and S is the probability of a radiationless transition.

Assuming a steady state condition, then the time derivatives are zero, and

$$\frac{N_2}{N_1} = \left(\frac{W_{13}\, S_{32}}{W_{31} + S_{32}} + W_{12}\right) \left(\frac{1}{A_{21} + W_{21}}\right) \tag{2.24}$$

Provided, $g_1 = g_2$,

$$B_{12} = B_{21}$$

and

$$W_{12} = W_{21}$$

If the radiationless transition from level #3 to level #2 occurs much faster than the radiative transitions to level #1, i.e.,

$$S_{32} >> W_{31} \; ; \; S_{32} >> A_{31}$$

Equation (2.23) becomes

$$\text{(a)} \quad 0 = W_{13}N_1 - S_{32}N_3$$

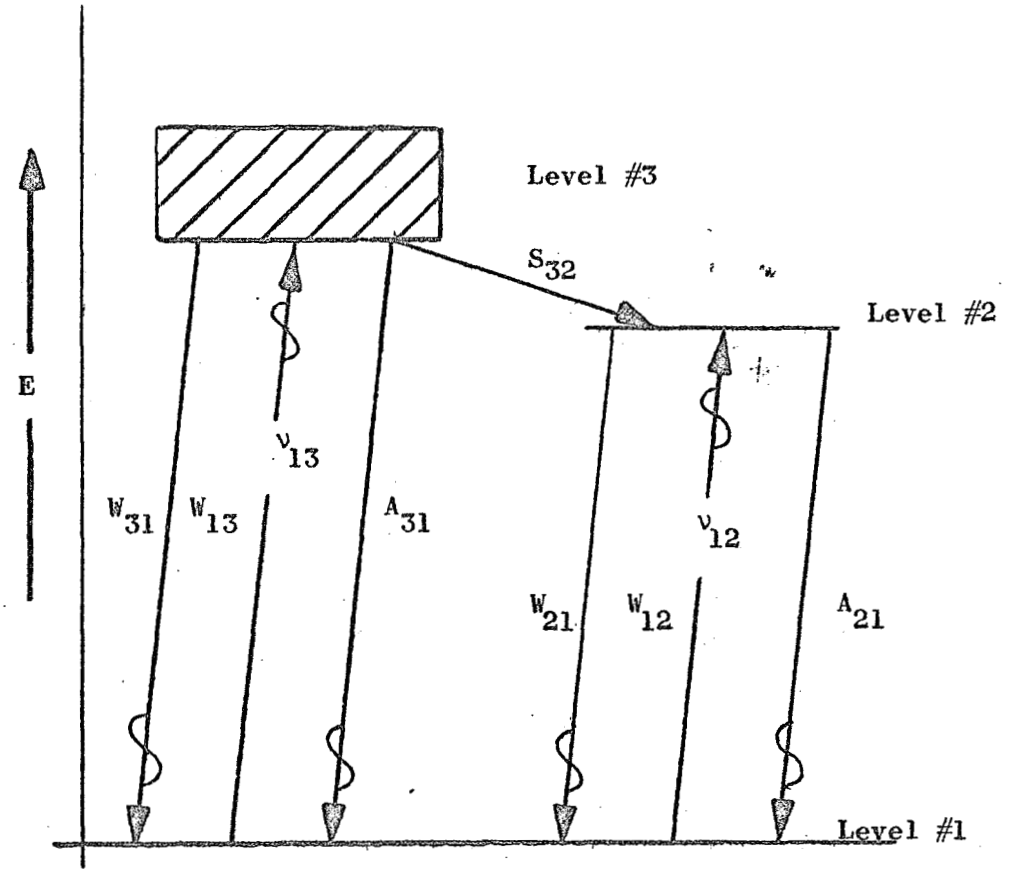

Figure 2.3. Energy Level Diagram of a Three Level Laser Medium.

$$(b)\quad 0 = W_{12}N_1 - (W_{21} + A_{21})\,N_2 + S_{32}N_3 \tag{2.25}$$

$$(c)\quad N_o = N_1 + N_2$$

Then, the following relation may be obtained,

$$\frac{N_2 - N_1}{N_o} = \frac{W_{13} - A_{21}}{W_{13} + A_{21} + 2W_{12}} \tag{2.26}$$

If the excitation is considered to be in the form of blackbody radiation, which completely engulfs the laser material,

$$W_{13} = \frac{g_3}{g_1}\, B_{31}\, u(\nu_{13}) \tag{2.27}$$

where ν_{13} = energy density of blackbody radiation of frequency ν_{13}. $u(\nu)$ is given by Plancks law,

$$u(\nu) = \frac{8\pi h\nu^3}{c^3}\,\frac{1}{e^{h\nu/kT} - 1} \tag{2.28}$$

for a vacuum. This becomes

$$u(\nu) = \frac{8\pi h\nu^3\eta^3}{c^3}\,\frac{1}{e^{h\nu/kT} - 1} \tag{2.29}$$

in a material with index of refraction η. The relation for B_{31} is

$$B_{31} = \frac{c^3 A_{31}}{8\pi h\nu_{13}^3\eta^3} \tag{2.30}$$

and this relation becomes

$$u(\nu_{13})\, B_{31} = \frac{A_{31}}{e^{h\nu/kT} - 1} \tag{2.31}$$

According to Equation (2.26), these inequalities must exist

$$W_{13} > A_{21} \text{ or } \frac{W_{13}}{A_{21}} > 1 \tag{2.32}$$

in order to obtain a population inversion, or light amplification. This condition requires that

$$\frac{g_3 A_{31}}{g_1 A_{21}} \geq e^{h\nu/kT} - 1 \qquad (2.33)$$

which can be solved for the minimum source temperature T_s. The solution is

$$\frac{g_3 A_{31}}{g_1 A_{21}} = e^{h\nu/kT_s} - 1$$

or

$$T_s = \frac{E_3 - E_1}{k \log (1 + g_3 A_{31}/g_1 A_{21})} \qquad (2.34)$$

This is the minimum temperature of a blackbody that is necessary to achieve population inversion. For a ruby, this temperature is in the neighborhood of 4,000°K.

As an illustration of the attainment of laser activity, consider a typical ruby laser. A typical arrangement is indicated in Figure 2.4. The main component of the ruby laser is the ruby. This is Al_2O_3 with a small amount of impurity, typically .05% by weight and usually Cr_2O_3. The aluminum and oxygen do not participate in the laser activity; only the chromium ions are responsible for the laser pulse. The most common source of excitation is a light pulse from either a helical, or a linear flashtube which is filled with some gas with a near continuum of spectral radiation. The flashtubes are powered by the energy that is stored in capacitor banks.

The energy level diagram of chromium ions in a ruby host contains a three level system that is capable of light amplification. Immediately after the initiation of the excitation pulse, spontaneous radiation, or fluorescence, begins and stimulated emission follows in approximately 0.5 milliseconds. The output from stimulated emission is near 6943 Å for chromium impurity in ruby.

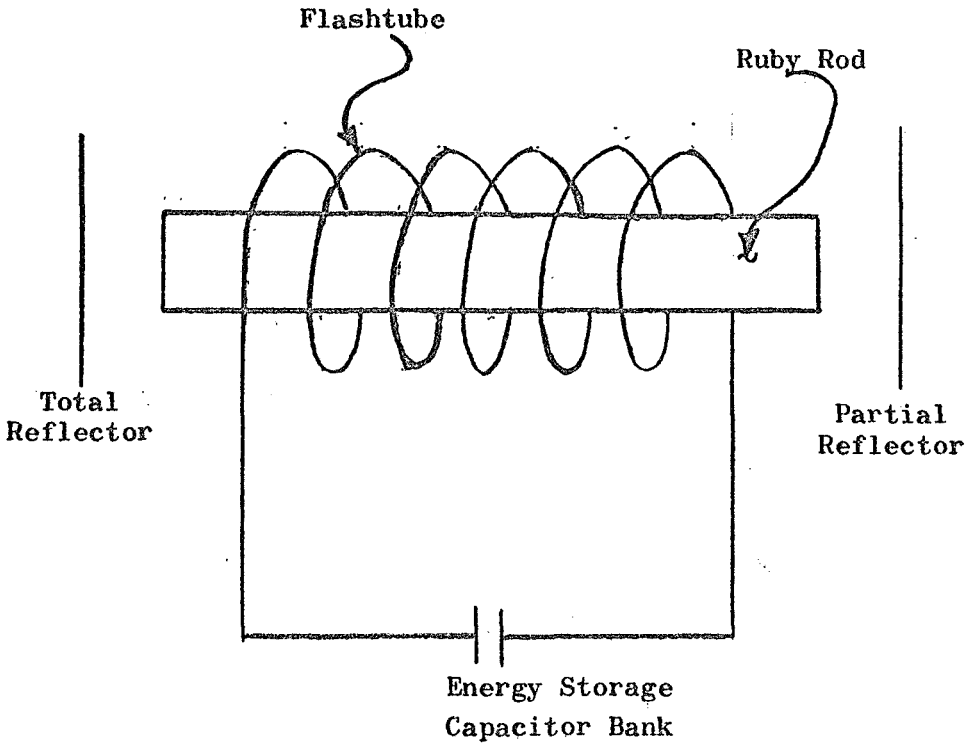

Figure 2.4. Schematic of a Typical Ruby Laser.

The purpose of the previous section was to provide the background and basis for a qualitative discussion of the ruby laser system that was assembled. It is not a general survey of lasers. Various aspects of the laser problem, such as line-width, moding, etc., have not been discussed since the primary interest in the laser system is as a means for obtaining a sharply defined, high power, light pulse. For more information on the topics which are not covered, the reader is referred to the references in the bibliography. The next section of this chapter deals with the technique of q-switching and the final section concentrates on the particular laser system which has been constructed.

Q-Switching

As discussed in the previous section, the onset of laser activity depends on the accumulation of sufficient excitation centers in the laser cavity by the absorption of radiation from the excitation source. This phenomena is the basis for a technique which is termed q-switching. With q-switching a well defined pulse is attained from the laser at power levels which are considerably larger than those in the conventional pulsed operation.

The output of a ruby laser, which is operated in the manner that is described in the previous section, consists of irregularly spaced, high frequency pulses. During excitation by the flashtube, the accumulated excitation centers are depleted by the light amplification process through these random light pulses of somewhat variable intensity. These pulses are designated as the regular operation of the laser and the variation in amplitude of the pulses indicates that the pulse does not always require the same accumulation of excitation centers in order

to be initiated. There is a random mechanism in the pulse initiation. These randomly spaced pulses are obtained for almost the entire duration of excitation of the ruby by the flashtube. There is a rough upper limit to the energy (ΔE) in each of the series of pulses, and the power level ($\Delta E/\Delta t$) that may be obtained.

The technique of q-switching consists of placing an absorber, whose absorbtance may be changed, within the laser cavity. If the laser cavity is considered as an amplifier which is tuned to resonance, the effect of the absorber is to "spoil" the q, or quality, of this cavity. This gives rise to the term "q-spoiling", which is sometimes used in lieu of "q-switching". Various types of absorbers have been employed for q-switches such as optically active dyes, Kerr cells, thin metallic films, and thin optically active films.

At a certain instant during the excitation, the q-switch is made transparent, or nearly so, which allows the laser cavity to achieve a negative absorption, or a state of amplification. On a microscopic scale, the effect of the q-switch is to prevent the depletion of excited states by stimulated emission. This permits the laser medium to continue to accumulate excitation, and to attain a high level of population inversion. This results in a greatly increased coefficient of amplification. When the absorption by the q-switch is removed, the population inversion is rapidly depleted by stimulated emission, which produces the giant laser pulse.

At some later point in time, the q-switch again becomes absorbtive and this leads to the termination of the laser pulse. The duration of the q-switched pulse, commonly termed a giant pulse, is controllable by the q-switch. By only permitting laser activity for a small

time, Δt, the power level of the output ($\Delta E/\Delta t$) is greatly enhanced over the level obtained by conventional operation. The total energy output, however, is reduced by q-switching.

A relative comparison of the q-switched and the conventional output is illustrated in Figure 2.5 (Lengyel, 1966).

Analysis of the Twin Ruby Laser

The preceding sections provide the reader with a review of the fundamental principles of the laser. The theoretical description of more sophisticated laser systems is a very complex problem and is beyond the scope of this thesis. For this reason, no attempt is made to provide a quantitative, theoretical analysis of the twin ruby laser system; instead, a qualitative discussion of the system is given in this section.

The description of a typical, twin ruby laser is readily started with descriptions of each item in the assembly. The necessary components consist of two flashtubes, two rubies, a q-switch and a partial reflector.. The arrangement of these components is indicated by the sketch in Figure 2.6. The two ruby rods are separated by a q-switch. The assembly is terminated by a partial reflector which is one side of an optical flat. The rubies are 0.5 inches in diameter and 6.0 inches long. Ruby #1 has one end cut to form a totally reflecting prism which serves as the total reflector in the cavity. The other end of the rod is faced at Brewster's angle for ruby. The q-switch consists of a quartz cell which is filled with cryptocyanine, an optically active dye. Ruby #2 has one end cut at Brewster's angle and the other end is polished to a plane surface. An optical flat serves as the output

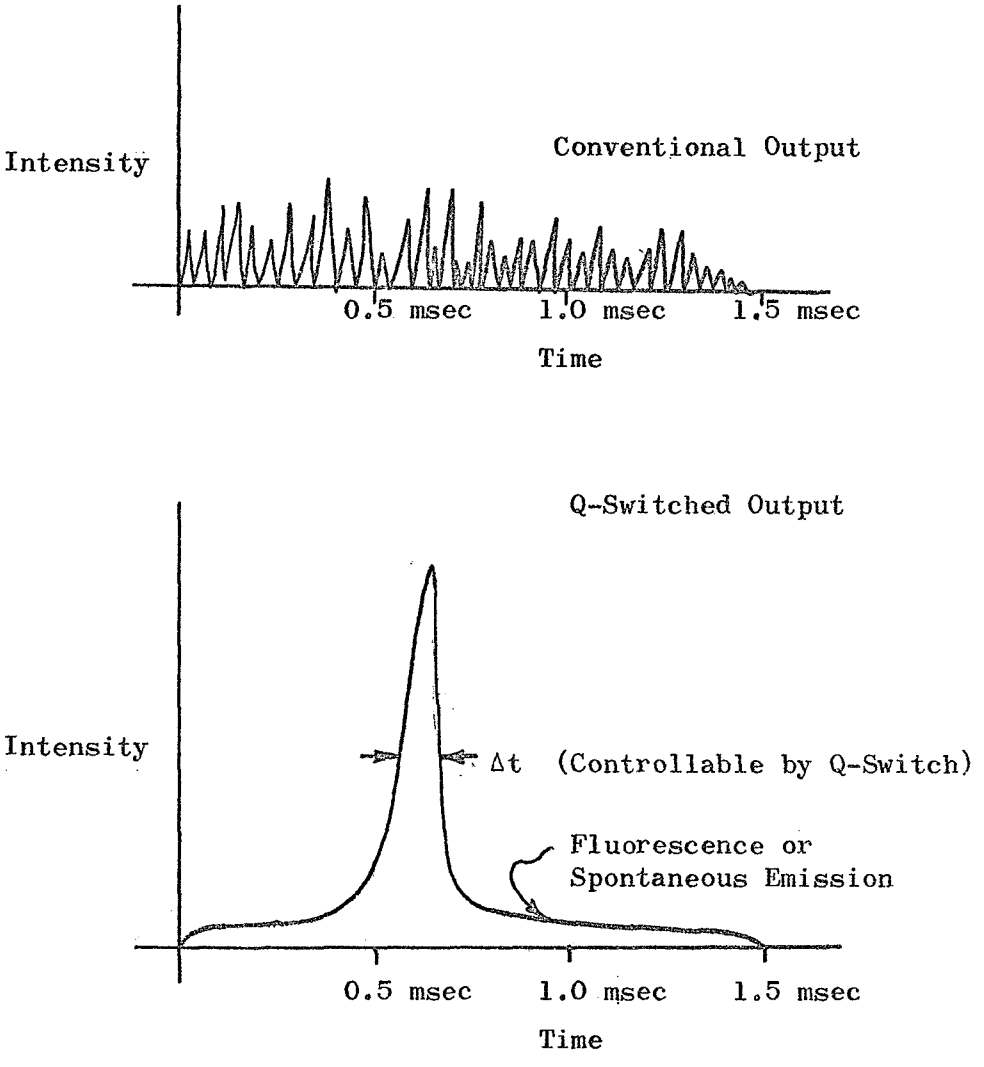

Figure 2.5. Comparison of Q-Switched and Conventional Laser Outputs.

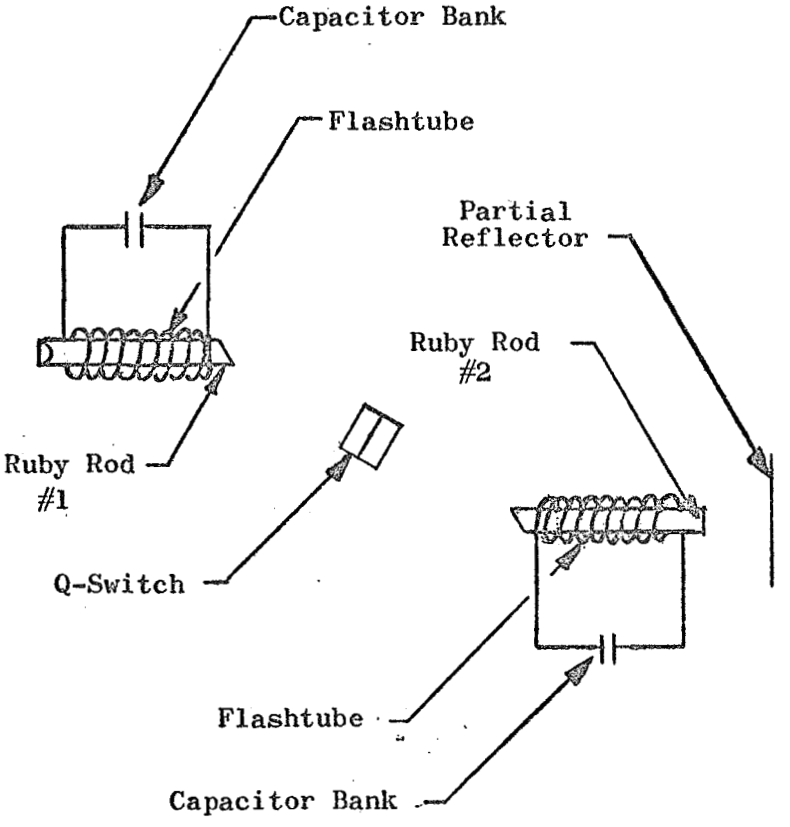

Figure 2.6. Twin Ruby Laser System.

reflector for the twin rod cavity. Each optical surface is flat to $\frac{1}{10}$ wavelength.

When the flashtubes are discharged, population inversion and spontaneous emission begin to occur in the rubies. In order for stimulated emission to occur, however, sufficient energy must be reflected back and forth within the ruby rods. This is prevented by the q-switch which is highly absorbtive at low light intensities. This permits the ruby rods to attain a large population inversion. As the inversion increases, the fluorescent light which is incident on the q-switch increases in intensity. At a certain intensity level, the absorbing centers in the q-switch become saturated so the absorbtion drops to zero. This allows the light to be reflected back and forth within the rods, giving rise to stimulated emission. Because of the higher reflectance of the totally reflecting prism, the cavity formed by the #1 rod and the shutter cell has a greater efficiency than the cavity of #2 rod. If both rods are in a state of population inversion, the pulse will originate in rod #1 and will be amplified on passing through the second rod. As the population inversion is reduced by the process of stimulated emission, the light intensity incident on the q-switch is decreased. At a certain intensity level, the q-switch will again become absorbtive, which terminates the laser pulse.

If the q-switch is not filled with cryptocyanine but is left in the cavity, the laser operates in the conventional sense. In this case, the output will again originate from the #1 rod because of the higher reflectances of the first cavity. This pulsating output will be amplified on passing through the second rod. For this reason, the first ruby rod will, in the remaining sections, sometimes be referred

to as the generating rod and the second rod will be referred to as the amplifier.

CHAPTER III

LASER DESIGN AND CONSTRUCTION

The design of the laser was based on the following criteria:

1. An output level which is in the order of 0.1 gigawatt.
2. A design which is compatible with the instrumentation presently employed in a light gas gun that is employed for particle impact studies.

The first requirement limits the choice of the laser medium and the pumping geometry. The second requirement results in some restrictions on the mechanical configuration of the system. The system, as it has been constructed, is described in the succeeding sections in relation to these two requirements and to the theory that is presented in the previous chapter.

Laser Cavity

In order to achieve the power and the energy levels that are required for the laser beam impact experiments, a q-switched ruby laser system with two rods in a generator-amplifier configuration was used. With this system, additional amplifier stages may be added if they become necessary. In addition, the system may be used in either a q-switched, or a conventional mode.

The laser rods were supplied by Linde Corporation. They have a chromium dopant level of 0.05% and have a matte finish on the barrel

of the rod. The beam divergence of the rods is specified as 0.5 milliradians, or less. In order to optimize coupling between the generating and amplifying rods, their mating faces have been cut at Brewster's angle for ruby. This enhances one polarization in the laser output and suppresses the other polarizations. The arrangement of the ruby rods and the other optical elements within the laser cavity is shown in Figure 2.6.

The ruby rod that is employed as a generator is 0.5 inches in diameter and 6 inches in length. It has a total internally-reflecting prism cut on one end, and the other is polished to the Brewster's angle. The amplifier, ruby rod is also 0.5 inches in diameter and 6 inches long. One end is faced at Brewster's angle and the other, the output surface, is polished optically flat.

The other two elements in the laser cavity are a passive q-switch and an optical flat. The q-switch consists of twin quartz optical flats, polished to a tolerance of $1/10\,\lambda$, and cemented paralled to each other at a separation of 1.0 mm. The cell is filled with an optically active dye, which is a solution of cryptocyanine in methanol (Kaflas, Masters, and Murray, 1964). Until a predetermined intensity of light level is reached, this dye remains absorbtive and prevents the cavity oscillation which is necessary for laser action. When the critical intensity is attained, the dye becomes transparent and the laser pulse is emitted. The optical flat is 2.5 inches in diameter and serves as a partially reflecting suface, 8%, which is required for laser action. This optical flat also serves as a window to the evacuated target enclosure.

Laser Excitation

The two laser rods are excited, or optically pumped, by means of two, helical, xenon flashtubes. These flashtubes operate from twin, energy-storage capacitor banks, with each having a capability of 26 kilojoules at 10,000 volts. Helical flashtubes were chosen to obtain a uniform distribution of the excited levels across the cross-section of the rubies. Linear flashtubes give a higher efficiency between the energy into the flash and the energy in the giant pulse but they do not give a uniform excitation across the cross-section of the ruby. If the more efficient, straight flashtubes were employed, a multi-elliptical enclosure would be required in order to focus the image of the flash into the region near the axis of the ruby. Since the diameter of the luminous discharge in the flashtube is smaller than the diameter of the ruby, the focused images of the flashtubes would not cover the entire cross-section of the ruby but only a region near the axis. The remainder to the ruby would be illuminated by the less intense light that converges from the surface of the ruby to the image that is near the axis. The choice of helical flashtubes also simplifies the design of the flashtube enclosures.

Each laser rod is fitted into a protective glass sleeve and is inserted in the helical flashtube. This mounting is illustrated by the cut-away drawing in Figure 3.1. Each flashtube is contained in a reflecting enclosure which is coated with magnesium oxide to maximize optical coupling between the rod and the flashtube. The mechanical design of these flashtube enclosures is discussed in more detail in the section which describes the alignment of the optical elements which compose the laser cavity.

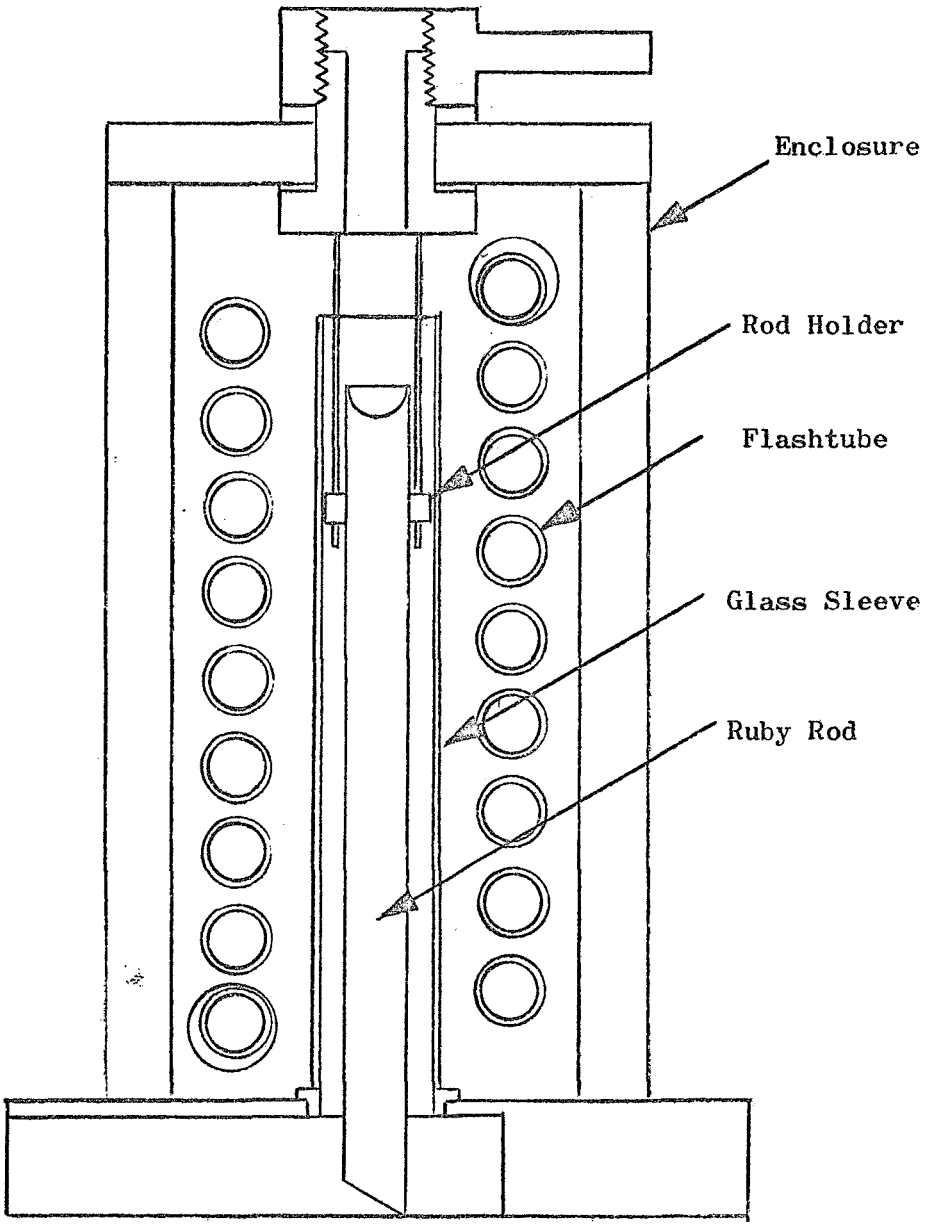

Figure 3.1. Flashtube Enclosure.

Each xenon flashtube is powered by a capacitor bank which stores 26 kilojoules at 10,000 volts. In order to obtain optimum optical pumping of the laser rods, the capacitor bank must discharge through the flashtube in a few milliseconds. The discharge circuit is a simple RLC series circuit. The resistance in the circuit is the flashtube resistance, nominally about 4.0 ohms. The circuit inductance is 80.0 microhenries and is due to the ballast inductor that is employed to shape the discharge. The capacitance is that of the storage banks, or 540.0 mircofarads. With these circuit values, the discharge current may be calculated as is indicated on the following pages.

The discharge obeys Equation (3.1), where q is the charge on the capacitor,

$$L\frac{d^2q}{dt^2} + R\frac{dq}{dt} + \frac{q}{C} = 0 \qquad (3.1)$$

This equation has the solution,

$$q = A_1 e^{-\left(\frac{R}{2L} + \sqrt{\frac{R^2}{4L^2} - \frac{1}{LC}}\right)t} + A_2 e^{-\left(\frac{R}{2L} - \sqrt{\frac{R^2}{4L^2} - \frac{1}{LC}}\right)t} \qquad (3.2)$$

Apply the boundary conditions, i.e., at $t = 0$,

$$q_o = CV_o = A_1 + A_2 \qquad (3.3)$$

and $\left.\frac{dq}{dt}\right|_{t=0} = 0$, which means that,

$$A_1\left(\frac{R}{2L} + \sqrt{\frac{R^2}{4L^2} - \frac{1}{LC}}\right) + A_2\left(\frac{R}{2L} - \sqrt{\frac{R^2}{4L^2} - \frac{1}{LC}}\right) = 0 \qquad (3.4)$$

Solve these two equations for A_1 and A_2,

$$A_1 = \frac{-A_2\left(\frac{R}{2L} - \sqrt{\frac{R^2}{4L^2} - \frac{1}{LC}}\right)}{\frac{R}{2L} + \sqrt{\frac{R^2}{4L^2} - \frac{1}{LC}}} \qquad (3.5)$$

and

$$A_2\left[1 - \frac{\frac{R}{2L} - \sqrt{\frac{R^2}{4L^2} - \frac{1}{LC}}}{\frac{R}{2L} + \sqrt{\frac{R^2}{4L^2} - \frac{1}{LC}}}\right] = CV_o \tag{3.6}$$

These become

$$A_2 = \frac{CV_o\left(\frac{R}{2L} + \sqrt{\frac{R^2}{4L^2} - \frac{1}{LC}}\right)}{2\sqrt{\frac{R^2}{4L^2} - \frac{1}{LC}}} \tag{3.7}$$

and

$$A_1 = -\frac{CV_o\left(\frac{R}{2L} - \sqrt{\frac{R^2}{4L^2} - \frac{1}{LC}}\right)}{2\sqrt{\frac{R^2}{4L^2} - \frac{1}{LC}}} \tag{3.8}$$

Insert the values for this equipment,

$$\begin{aligned} R &= 4\Omega \\ L &= 80\ \mu h \\ C &= 540\ \mu f.; \end{aligned} \tag{3.9}$$

hence,

$$A_1 = -.0096\ CV_o \tag{3.10}$$

and

$$A_2 = 1.0096\ CV_o \tag{3.11}$$

The voltage on the capacitor bank is given by,

$$V_{cap} = V_o\ (1.0096e^{-500t} - .0096e^{-5.3x10^4 t}) \tag{3.12}$$

and is plotted in Figure 3.2. The flashtube current and the power dissipated in the flashtube as a function of time are calculated below,

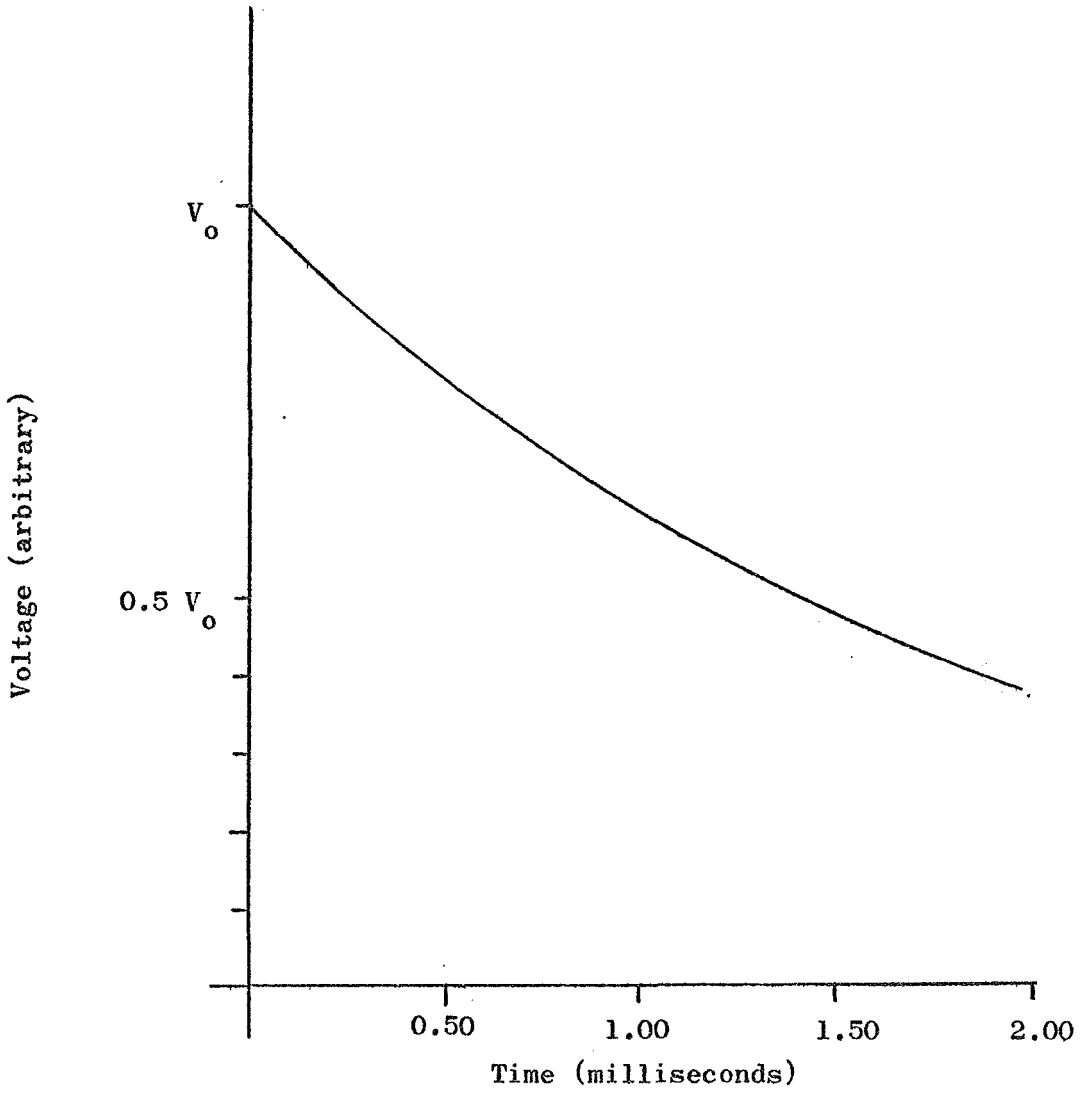

Figure 3.2. Capacitor Bank Voltage as a Function of Time.

$$V_{fl} = \frac{dq}{dt} R = RI_{fl} \tag{3.13}$$

$$I_{fl} = (506e^{-5.3x10^4 t} - 506e^{-500t})\, CV_o \tag{3.14}$$

or

$$I_{fl} = .256\ (e^{-5.3x10^4 t} - e^{-500t})\ V_o \text{ (amps.)} \tag{3.15}$$

$$V_{fl} = 1.024\ (e^{-5.3x10^4 t} - e^{-500t})\ V_o \text{ (volts)} \tag{3.16}$$

and finally

$$P_{fl} = I_{fl}V_{fl} = .262\ (e^{-5.3x10^4 t} - e^{-500t})^2\ V_o^{\,2} \text{ (watts)} \tag{3.17}$$

Equations (3.15) and (3.17) are displayed graphically in Figures 3.3 and 3.4, respectively.

Assume the flashtube to be a blackbody which radiates power at the same rate at which electrical power is supplied; then

$$P_{rad} = \text{power radiated} = \sigma AT^4 \tag{3.18}$$

where A = flashtube surface area $\cong .130\ m^2$

Use P_{fl} from Equation (3.17),

$$P_{rad} = \sigma AT^4 = P_{fl} \tag{3.19}$$

or

$$\sigma AT^4 = .262\ (e^{-5.3x10^4 t} - e^{-500t})^2\ V_o^{\,2}$$

then

$$T = \frac{.262}{\sigma A}^{1/4} (e^{-5.3x10^4 t} - e^{-500t})^{1/2}\ V_o^{\,1/2} \tag{3.20}$$

Equation (3.20) is shown graphically in Figure 3.5, for two values of V_o. Reference to Equation (2.34), shows that the flashtube pulse is sufficient for laser activity.

As a consequence of limited floor space and as an added safety factor, the energy storage banks were suspended from the ceiling. They

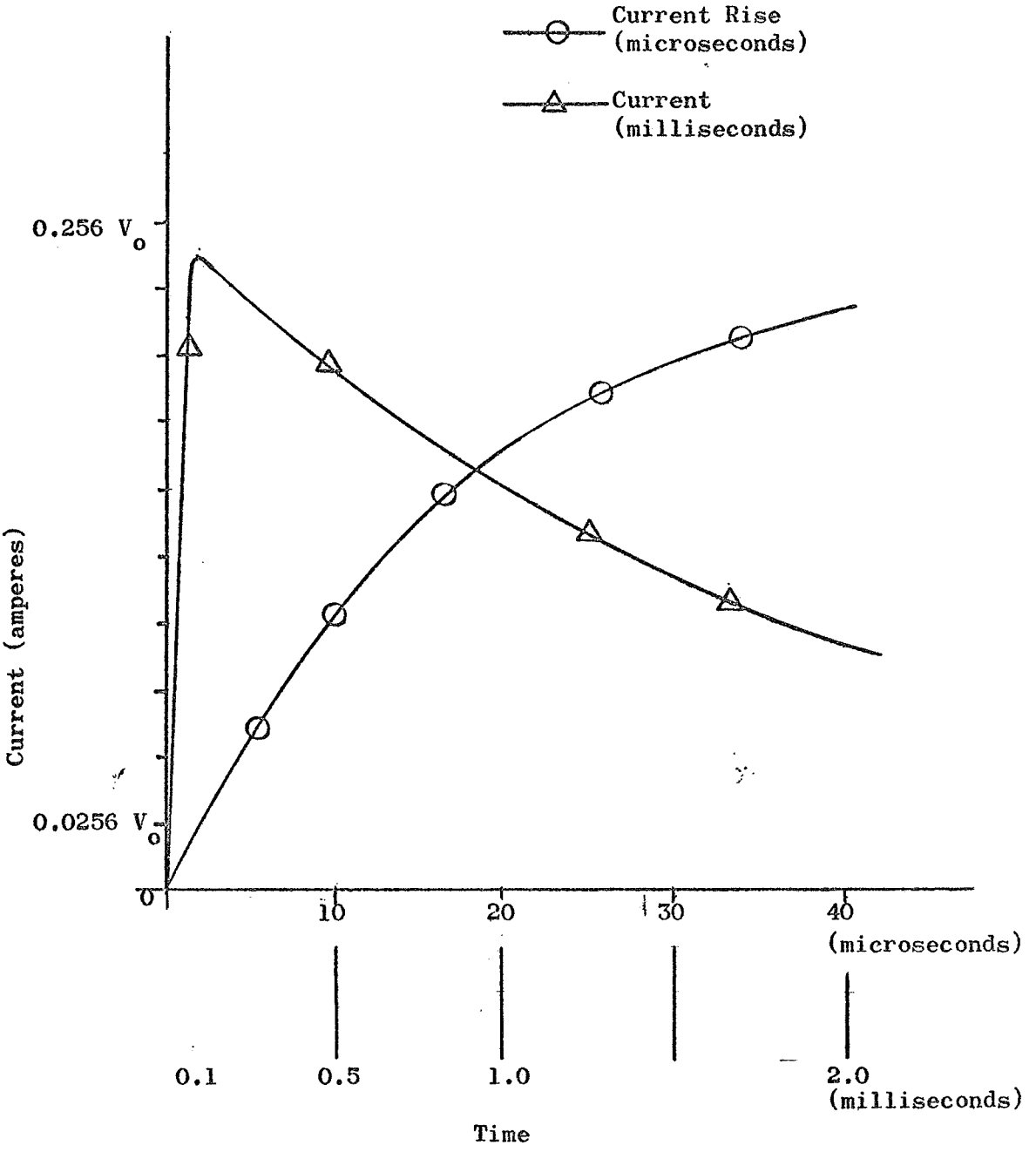

Figure 3.3. Flashtube Current as a Function of Time.

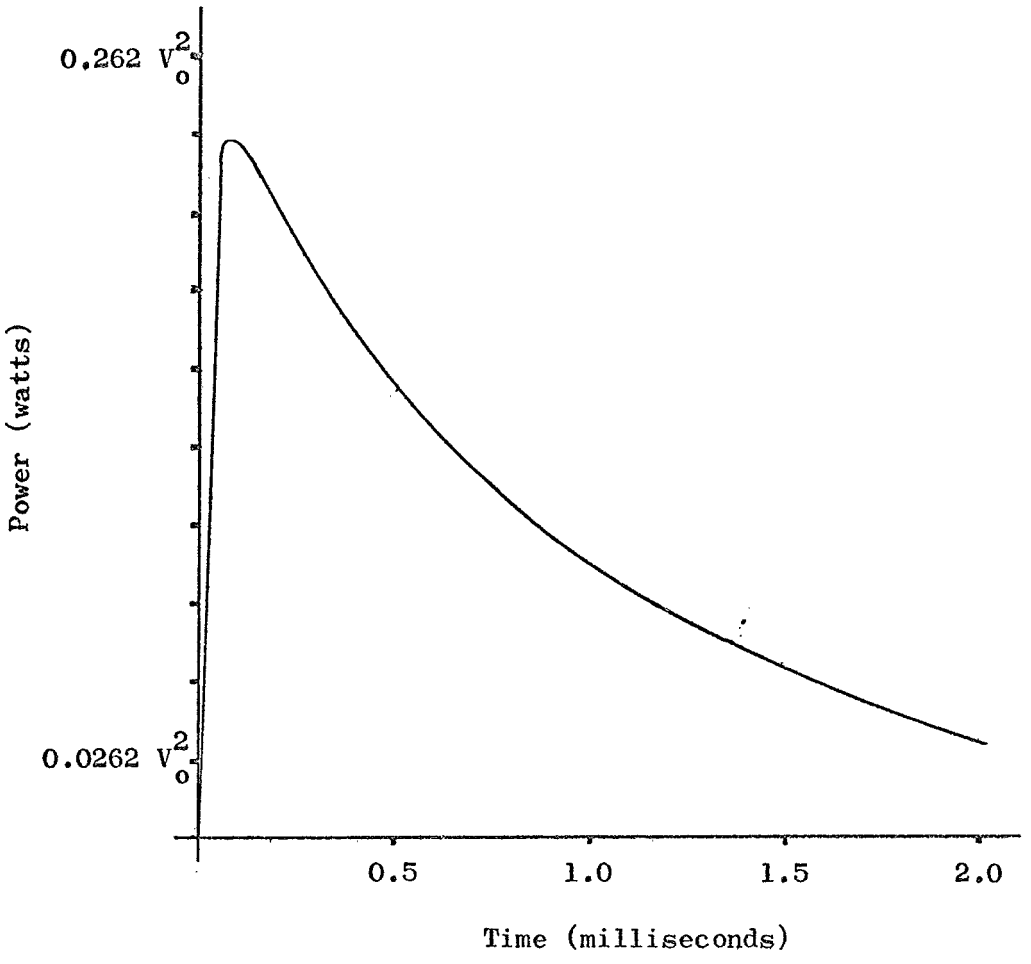

Figure 3.4. Flashtube Power as a Function of Time.

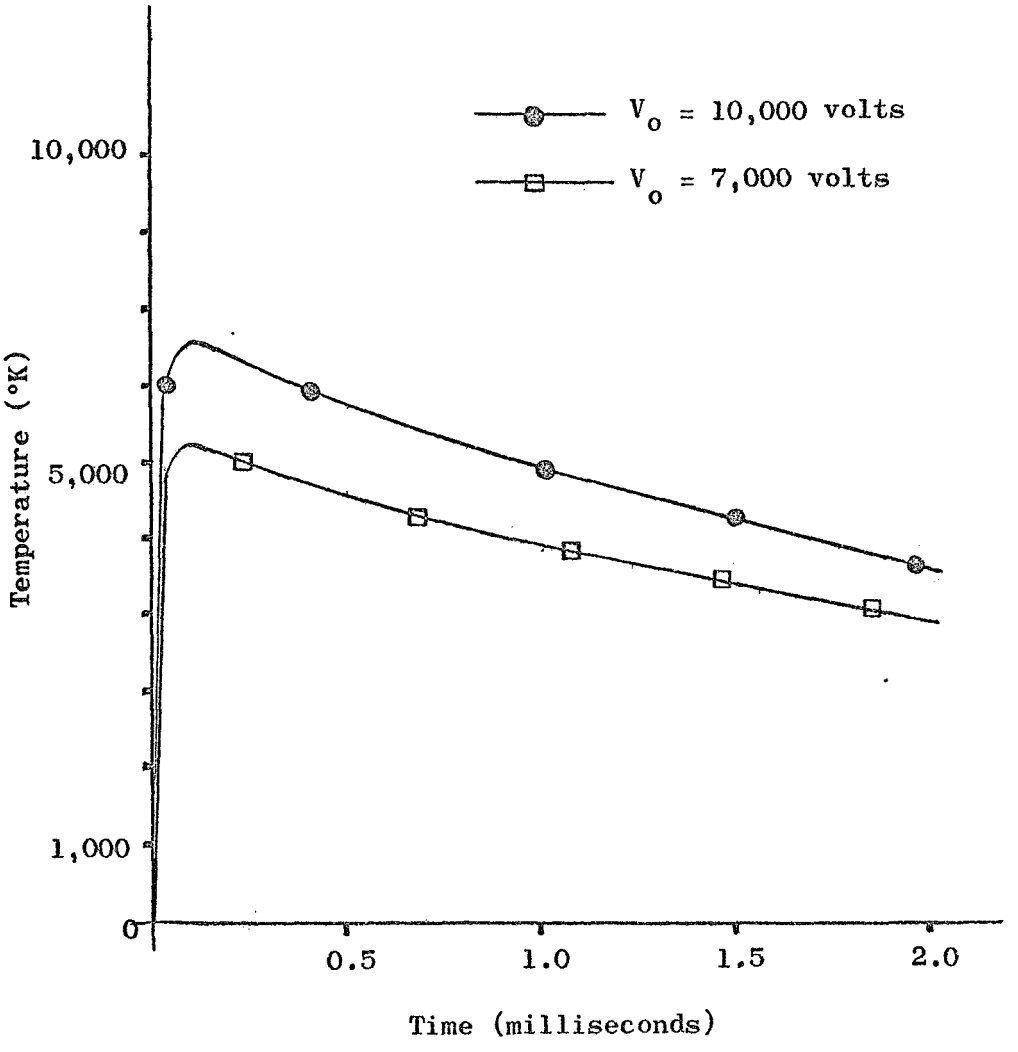

Figure 3.5. Flashtube Blackbody Temperature as a Function of Time.

are seen in the photograph of the system in Figure 3.7. The banks are charged by a 10,000 volt, DC power supply which is available in the laboratory. The twin banks are connected in a series-parallel arrangement so they may be charged simultaneously, with a charging time of 30 minutes. This insures that both banks will discharge in the event of a failure.

Because of the nature of the xenon flashtubes, the banks are fired by means of 50:1 pulse transformers which are supplied by Kemlite Corporation. The flashtubes are, in essence, spark gaps which are capable of withstanding 10,000 volts. They are fired by means of a trigger pulse through the primaries of the two parallel-connected pulse transformers. The voltage which is induced in the secondary of each pulse transformer is applied to a trigger lead. This lead is a single turn of molybdenum wire around the flashtube. This pulse initiates an arc within the flashtube which is sustained between the electrodes by the capacitor bank. The parallel connection of the pulse transformer primaries was to provide simultaneous pulsing of the flashtubes. The complete electrical circuitry is shown in the schematic of Figure 3.6.

Laser Alignment

The elements in the laser cavity, i.e., the two ruby rods, q-switch and output flat, must be carefully aligned. The tolerance for this alignment is determined by the beam divergence of the ruby rods. For the available components this tolerance is 0.5 milliradians or 0.03 degrees. Since it was accessible, the plane output surface of the amplifying rod was taken as the reference and the other elements were aligned with this surface. The alignment was accomplished by adjustment of

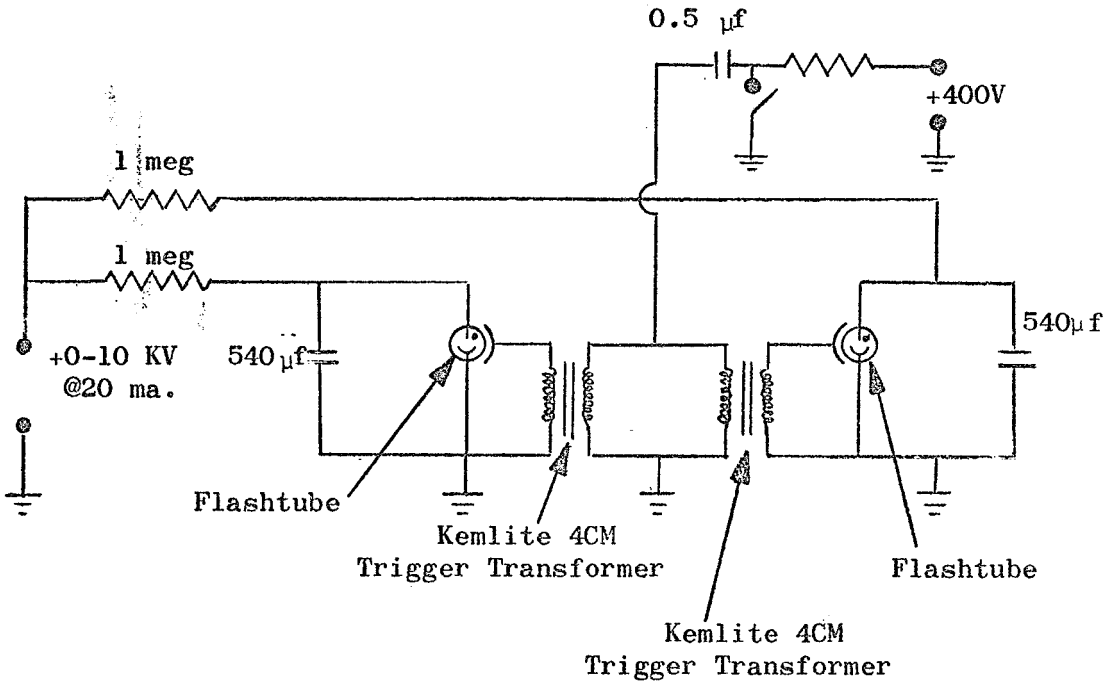

Figure 3.6. Schematic of Flashtube Circuit.

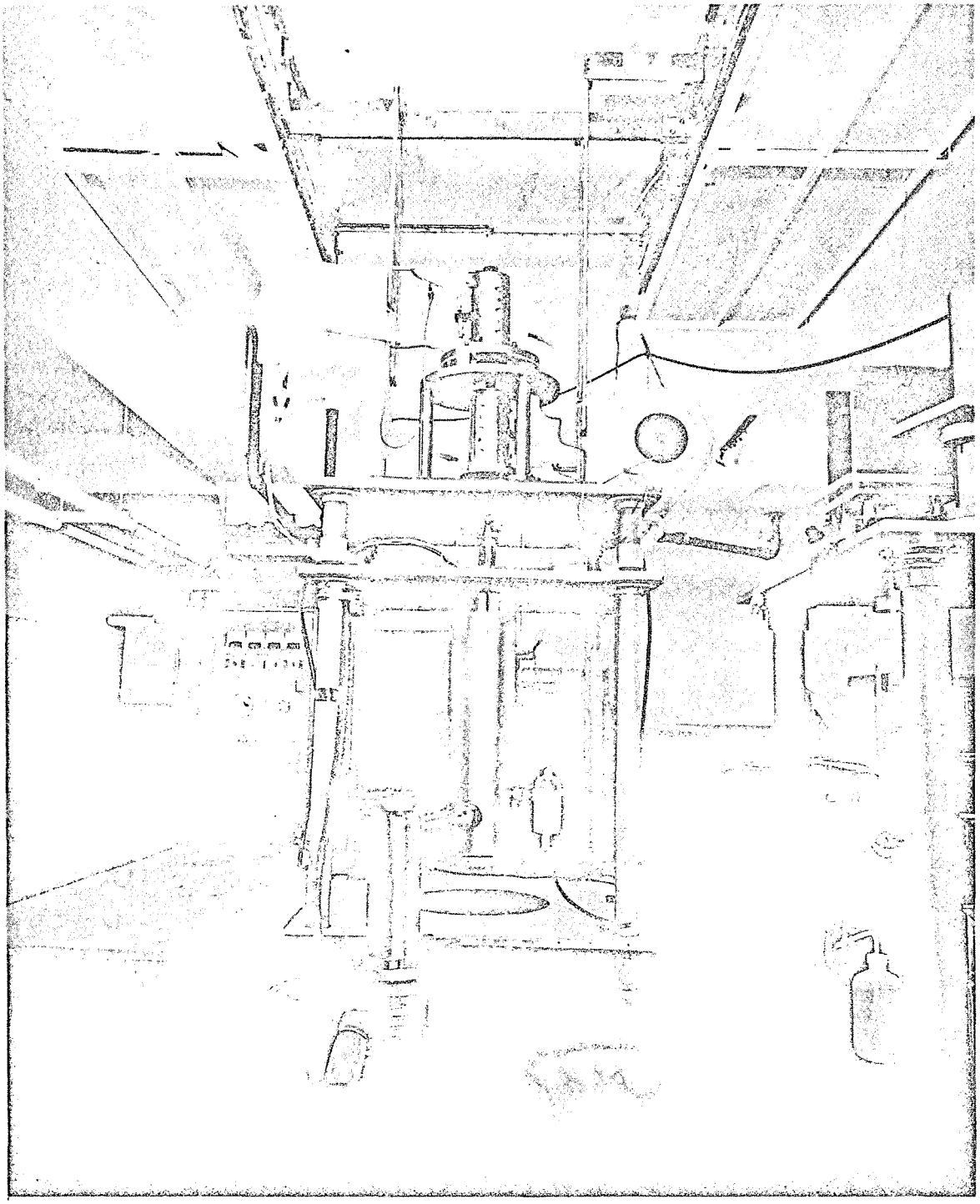

Figure 3.7. Photograph of Laser Facility.

differential screws and was monitored by optical methods. The alignment mechanisms and the optical checks are described in this section.

In order to obtain as much relative stability between the components as is possible, all items for the twin ruby laser are mounted with respect to a heavy reference plate, or platform. Only one component, the "partial reflector" in the sketch, Figure 2.6, is not attached directly to this platform. The platform is supported on three legs in order to obtain clear space above and below it for attaching the components. The arrangement is indicated by the photograph in Figure 3.7. The amplifying rod enclosure is suspended below this platform and is mounted in a fixed position without adjustments. The shutter cell is contained in an adjustable mounting which is mounted in an enclosure atop this platform. The generating rod enclosure is mounted atop the shutter cell enclosure through a system of differential screws and adjustment pads. Finally, the optical flat is contained in a mount that is suspended beneath the amplifier module by three differential screws. Since the position of the flat must be adjustable and since it serves as a window to the evacuated target enclosure, it is coupled to the target enclosure by means of a bellows.

In order to simplify the description of the various adjustments and their function, the alignment procedure is described in the step by step procedure by which it is actually accomplished in practice. Several methods of checking the alignment of the various optical elements have been employed. All of these employ auto-collimation or auto-reflection as a means of checking the alignment. The following discussion describes one of these methods and serves to illustrate the

principles that are employed in the alignment procedure. The steps in the alignment process are summarized below.

1. Alignment of a collimated beam normal to the plane output surface.
2. Alignment of the generating rod within the beam path of the amplifying rod.
3. Installation and alignment of the shutter cell between the two rods.
4. Alignment of the optical flat.

In the first step, a parallel beam of light is obtained by use of a point surface lamp and a plano-convex lens, or by means of a gas laser. This beam is incident on a beam splitter which divides the beam into two mutually perpendicular components. One component is projected past a reticle and onto the plane output surface. Here it is reflected back past the reticle and onto a ground glass plate. This is shown schematically in Figure 3.8.

Two images of the reticle will appear on the ground glass plate. By adjustment of the beam splitter, these images can be made to coincide. When this occurs, the beam is normal to the output surface of the amplifying rod.

The accuracy of the adjustment outlined above, as well as the alignment accuracy of the other elements, depends on the accuracy of the auto-collimating system shown in Figure 3.8. The resolution of the auto-collimating system can be estimated in the following way. Define the constants,

d = optical path, distance from the reticle to the ground glass.

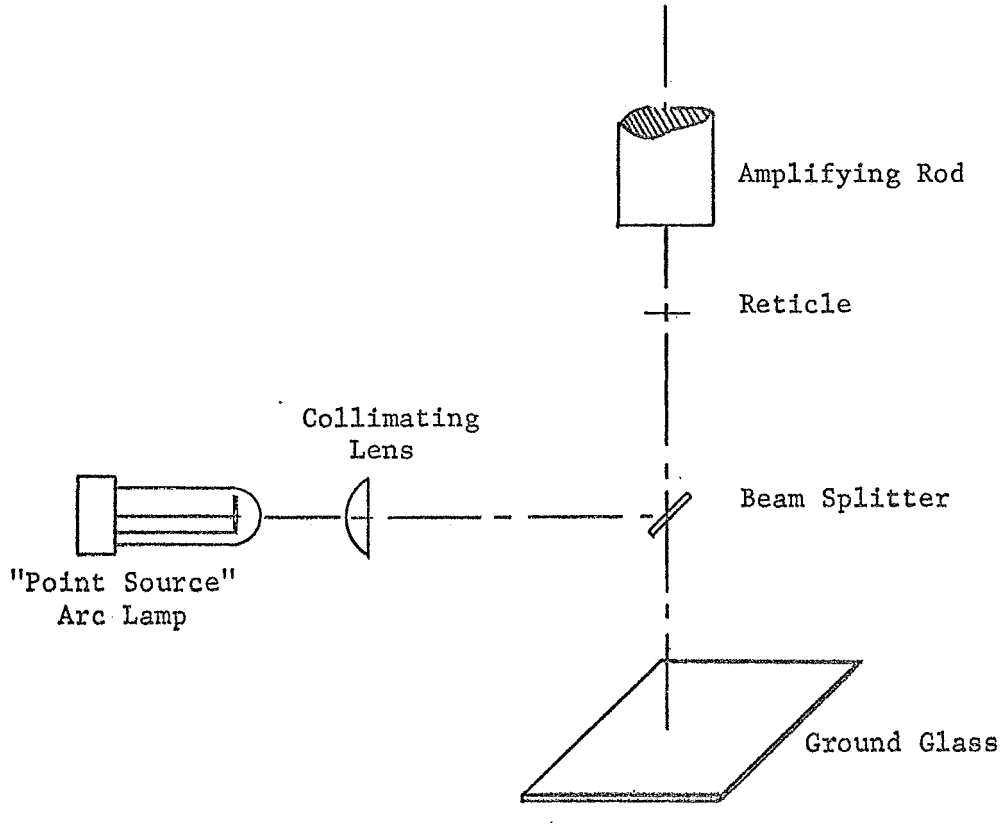

Figure 3.8. Schematic Drawing of Alignment Optics.

s = thickness of reticle wire.

Insert the values for these constant, d = 20 cm. and s = 1 mil. If 1 mil visual resolution is assumed,

$$1 \text{ mil} = d\theta$$

where θ is the accuracy of angular alignment, or

$$\theta = 0.1 \text{ milliradian}$$

which is well within the tolerance of beam divergence. For the other elements, the optical path is greater, and the accuracy of alignment is much better.

The next step in the alignment procedure, is the positioning of the generating rod in the beam that is projected through the amplifying rod. The auto-collimation set-up for this adjustment is the same that is shown in Figure 3.8. The beam of light, which carries the image of the reticle, is normally incident on the amplifying rod, projected through it and into the generating rod. At the totally internallly reflecting prism at the end of the generating rod, the beam is reflected back through the two ruby rods, past the reticle and viewed at the ground glass plate. The two images of the reticle are made co-linear by adjustment of a series of differential screws.

All of the differential screws that are mentioned in this chapter are a combination of 1/2-28 and 3/8-27 threads. With this combination, a movement of 0.001 inch is achieved. In all of the situations where differential screws are used, a cantilever arrangement is utilized. This cantilever arrangement insures a minimum of backlash in the adjustments. A sectioned drawing of a typical differential screw is presented in Figure 3.9.

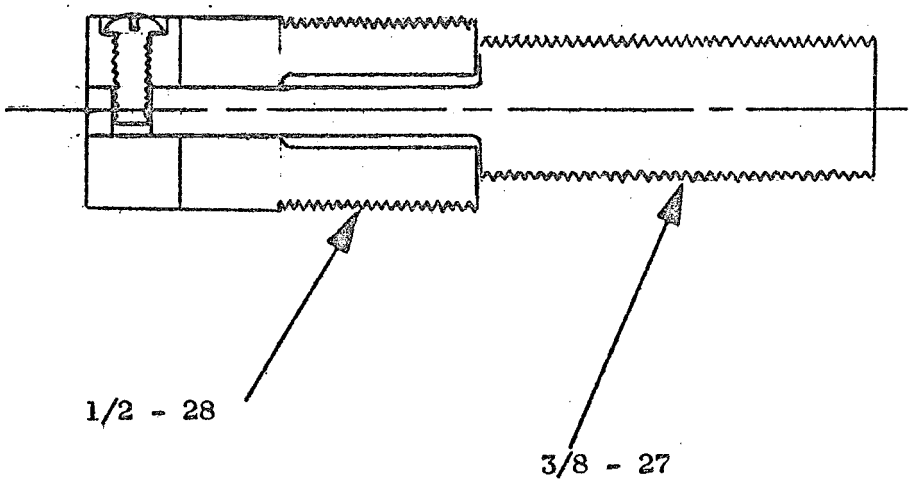

Figure 3.9. Differential Screw.

Since the amplifying rod is fixed, the generating rod enclosure must be capable of rotation about the vertical and horizontal axis, and also of transverse motion in two directions. The rotation about the vertical axis is accomplished by movement of an arm that is connected to the generating rod holder. The rotations about axes in the horizontal plane are made by a series of adjustments to three differential screws. These screws are threaded through the base of the generating rod enclosure and into a transverse adjustment block. It should be noted that the height of the generating rod enclosure can also be changed by means of these three screws. The transverse movements are controlled by means of four differential screws, two for each degree of freedom. Two screws are threaded through a block which is secured to the platform, and the screws are threaded into an L-shaped block. This provides one degree of freedom. The other movement is made by means of two screws that are threaded through the other leg of the L and into the transverse adjustment block to which the generating rod enclosure is attached. Both the L and the base are mounted on hardened steel balls to reduce friction. These adjustments are depicted in Figure 3.10.

The third step in the alignment procedure is to adjust the shutter cell in order to make it normal to the beam between the two rods. The optical check of Figure 3.8 is also employed for this step. The shutter cell, which is contained in an adjustable mount, is inserted into its housing between the two rods. Since the rods are aligned, any misalignment in the shutter cell is detected by observing the reticle images on the ground glass plate. The images are made co-linear by adjustment of the twin differential screws which push against a pivot

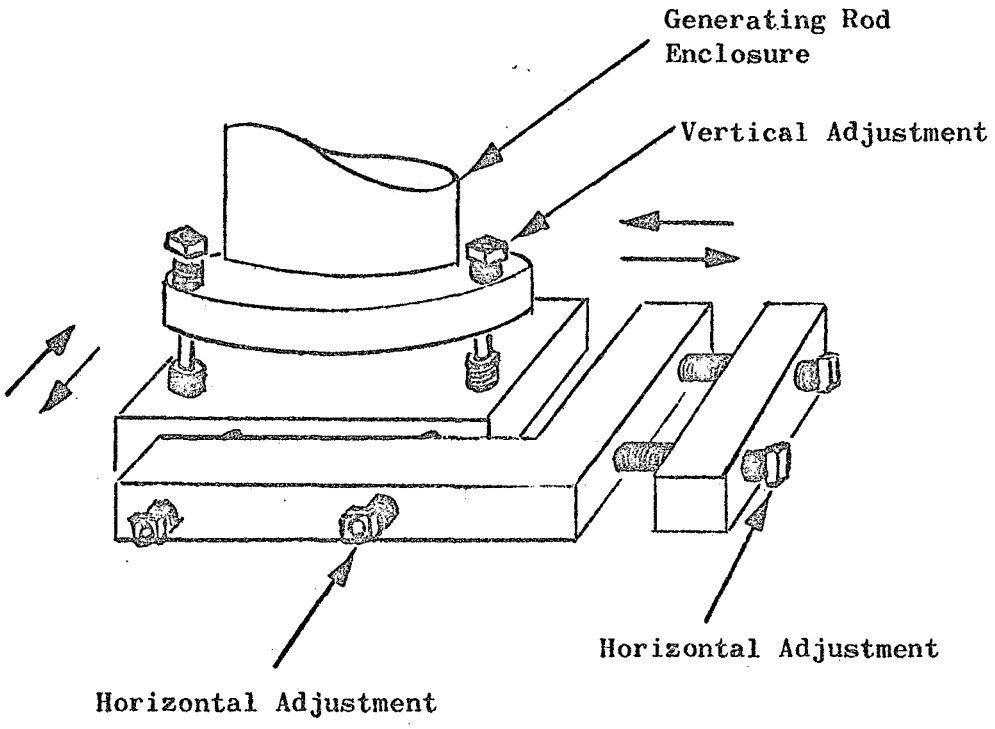

Figure 3.10. Generating Rod Adjustments.

arm. This cantilever arrangement and shutter cell mount is shown in Figure 3.11.

The final step in alignment is the adjustment of the optical flat in order to make it parallel to the output surface of the amplifying rod. This alignment is made by adjustment of the three differential screws which attach the optical flat mount to the amplifying rod enclosure.

Target Enclosure

The target in the initial experiments was aluminum in the shape of a disk with varying thicknesses. This target is mounted in an evacuated enclosure which also contains a plano-convex lens to focus the laser beam, and a "rat's nest calorimeter" to monitor beam energy. The target enclosure also contains a phototube to monitor the beam intensity as a function of time.

The vacuum system is fabricated of steel and is nickel plated to prevent corrosion. The system is pumped by means of a 6-inch diffusion pump, backed by a roughing pump. In addition, a cold trap is provided for high vacuum operation. The vacuum system, beam monitoring apparatus, and target are illustrated in the cut-away drawing of Figure 3.12.

The vacuum system is designed to be mated with a vacuum ultraviolet spectrograph that is available in the laboratory by means of a coupling port at the level of the target. This coupling port may also be used for photographic studies of the plasma which is associated with laser beam impact.

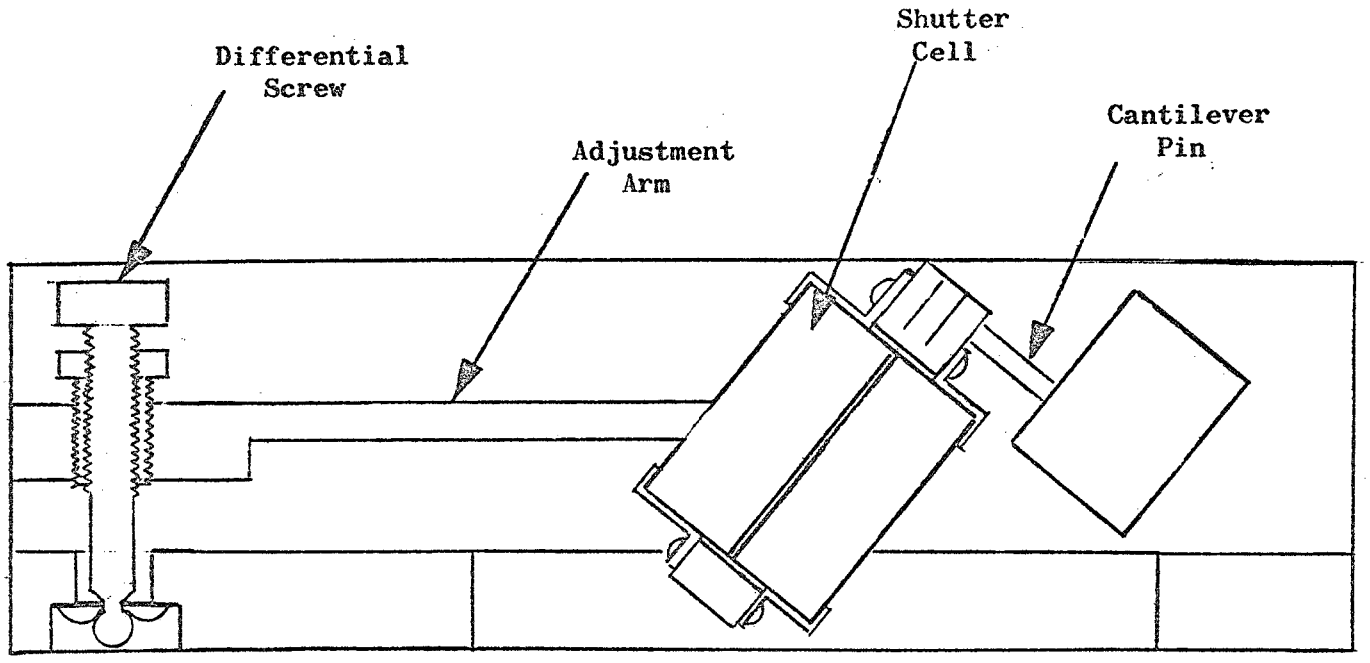

Figure 3.11. Shutter Cell Mount and Adjustments.

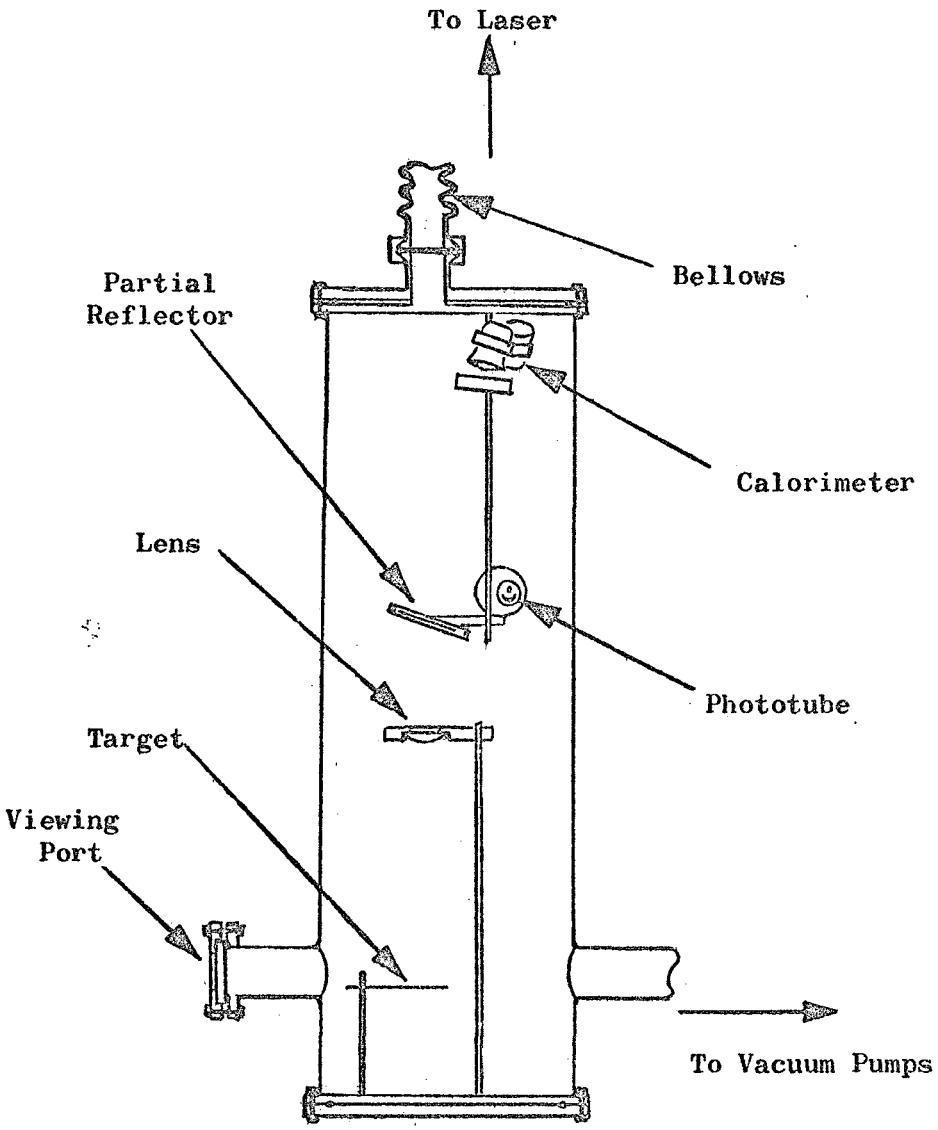

Figure 3.12. Cut-Away Drawing of Target Enclosure.

CHAPTER IV

INSTRUMENTATION FOR EXPERIMENTS

At the present time, the instrumentation for the laser facility consists of a beam monitoring device and a vacuum ultraviolet spectrograph. Time exposure photographs are to be obtained of the plasma that is ejected by the target as a result of the laser beam impact. Future studies, which are now in various stages of planning and construction, are to utilize a quadrupole mass filter and possibly a gas laser apparatus to measure electron density. In addition, the target deformation may be investigated by a metallograph which is available in the laboratory. Some of these devices, and the experiments for which they are planned, are described in this chapter.

Beam Monitoring

In order to evaluate the laser system and to facilitate future experiments, it is necessary to obtain some information about the laser output as a function of time, and its dependence on several system parameters. In order to obtain these measurements, a beam monitoring device has been constructed. The device consists of a phototube, two partial reflectors, and a rat's nest calorimeter (Baker, 1963). The entire package is contained in the target enclosure.

The laser beam is incident on partial reflector, #1, which is shown in Figure 4.1, at near normal incidence. Approximately 8% of the

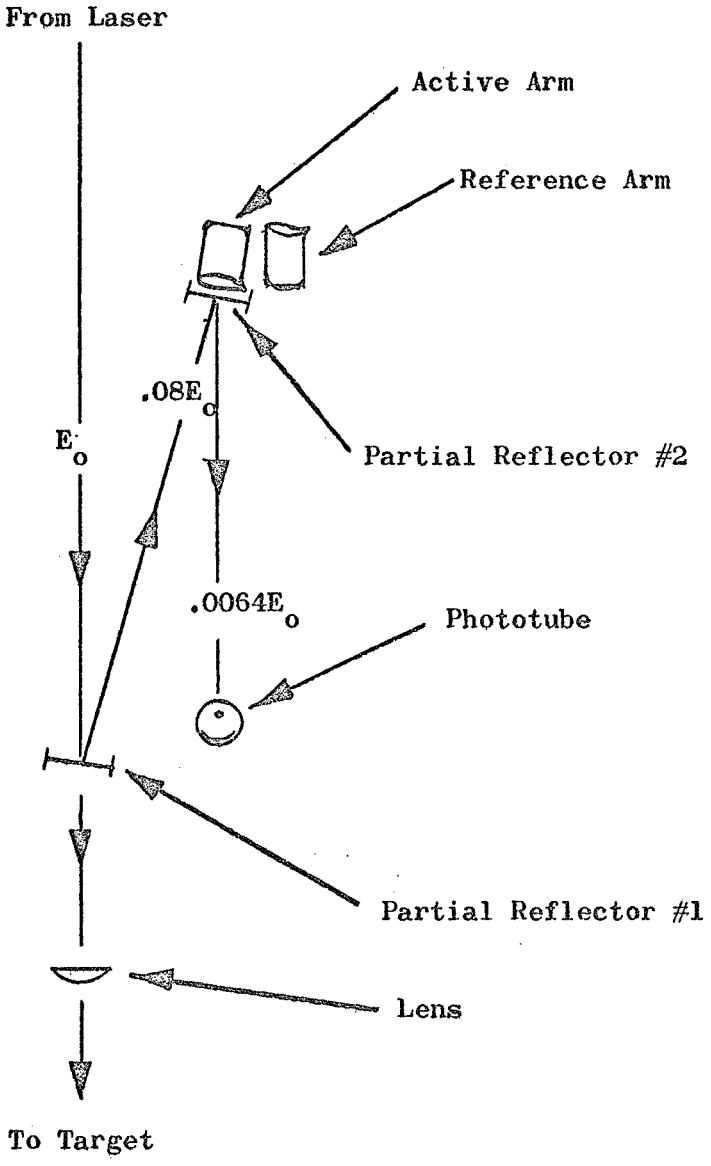

Figure 4.1. Rat's Nest Calorimeter and Phototube.

incident beam is reflected onto the glass plate (partial reflector #2) which is in front of the active arm of the rat's nest calorimeter. Of the incident light on this second glass plate, 92% enters the calorimeter, and the remaining 8% is reflected into the phototube. If the laser beam has an intensity I_0 (t) at a time, t, the intensity into the rat's nest calorimeter is 0.074 I_0. Similarily, the light incident on the phototube is 0.0064 I_0. The phototube provides a trace of the laser output as a function of time on an oscilloscope. A Tektronics Model 519 oscilloscope is available to provide a very short time resolution if it is required.

The rat's nest calorimeter provides a means of determining the total energy that is emitted by the laser. It is composed of two arms, an active arm and a reference arm. The two arms are identical except the reference arm receives none of the laser output. Both arms are contained within the target enclosure to insure the same environment. Each arm of the rat's nest calorimeter consists of a large length of small gauge, enameled copper wire which is stuffed at random into a small beaker to which a reflecting coating of MgO has been applied. This coating minimizes losses in the active arm and prevents light from entering the inactive arm. When light enters the active arm, it is absorbed by the copper wire, thereby raising its temperature. As a consequence, the total resistance of the arm increases. This resistance change is measured by means of the bridge circuit that is illustrated in Figure 4.2. The relation between the change of resistance and the absorbed energy is developed in the following paragraphs for the particular parameters of this calorimeter.

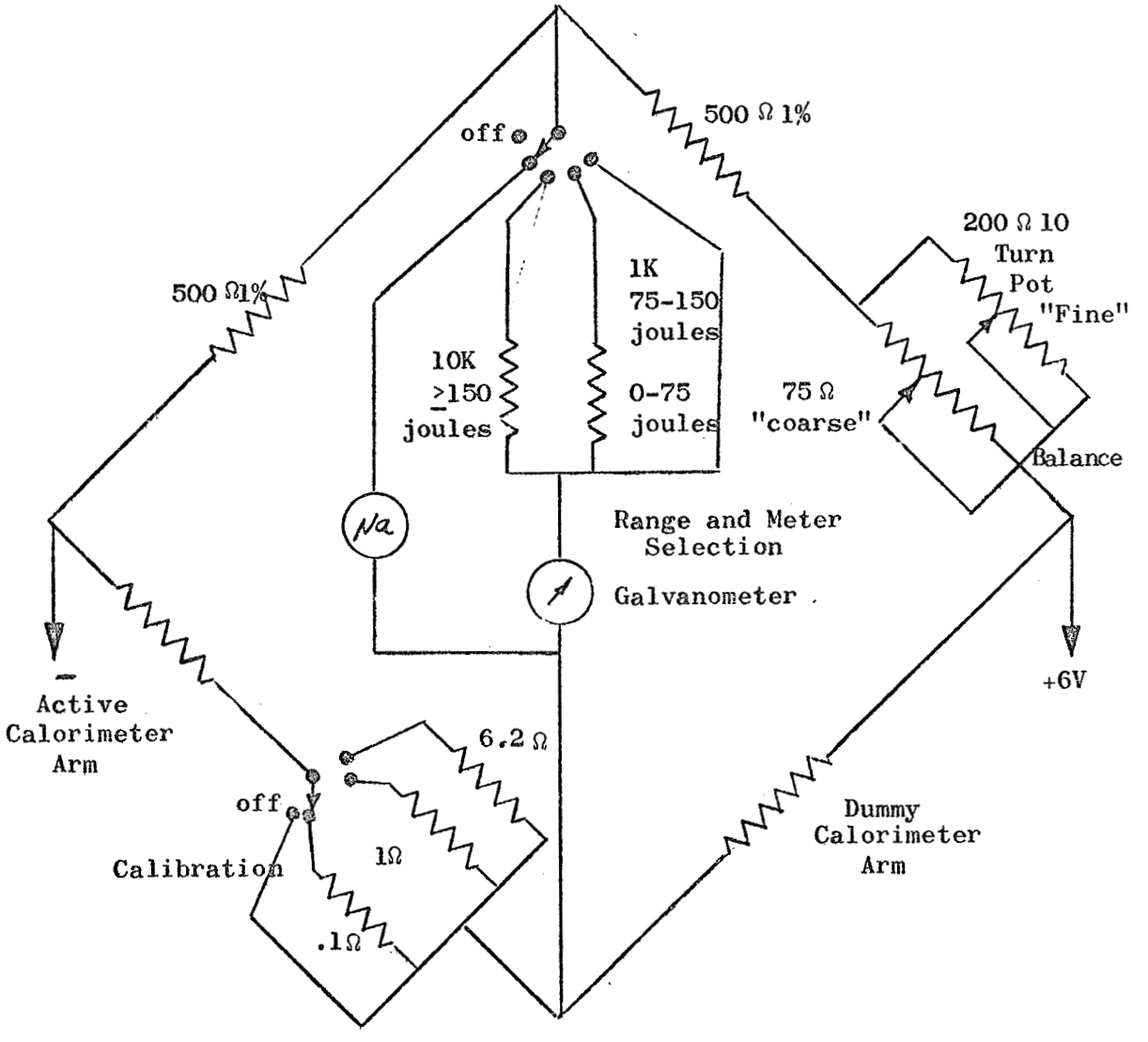

Figure 4.2. Calorimeter Bridge Circuit.

Take the resistance of the active arm to be R_0 before the laser pulse is incident, then the resistance change is

$$(R - R_0) = R_0 \alpha \, (T - T_0) \tag{4.1}$$

where

α = thermal coefficient of resistivity

R_0 = initial resistance

R = final resistance

T_0 = initial temeprature

T = final temperature

The temperature change is related to the energy, E, that is absorbed by the calorimeter by the relation,

$$E = Mc \quad (T - T_0) \tag{4.2}$$

where

M = mass of active arm

c = specific heat of the active arm.

Combine these two relations into

$$R - R_0 = \frac{R_0 \alpha \, E}{Mc} \quad . \tag{4.3}$$

Denote r_0 as the resistance/unit length and m as the mass/unit length, then

$$\frac{r_0}{m} = \frac{R_0}{M} \quad . \tag{4.4}$$

The product, mc, for the active arm is actually the sum of mc for the copper wire and mc for the insulation,

$$mc = (mc)_{wire} + (mc)_{insulation} \quad . \tag{4.5}$$

Hence, Equation (4.3) becomes

$$E = \frac{(R - R_0)\,[(mc)_{wire} + (mc)_{insulation}]}{r_0\,\alpha} . \qquad (4.6)$$

For #36 copper wire, the numerical constants are

$$r_0 = 0.432\ \Omega/ft. \qquad (4.7)$$

$$= 0.0039/°C$$

$$m_{insulation} = 1.385 \times 10^{-3}\ gm/ft$$

$$m_{copper} = 36.0 \times 10^{-3}\ gm/ft$$

$$c_{insulation} = 0.40\ cal/gm-°K$$

$$c_{copper} = 0.092\ cal/gm-°K .$$

With these values, the relation is,

$$E = 2.30\ (R - R_0)\ cal/\Omega \qquad (4.8)$$

or

$$E = 9.61\ (R - R_0)\ joules/\Omega . \qquad (4.9)$$

This is a relation for E, the energy which enters the calorimeter, and it must be modified to find a relation between E and the total laser beam energy, E_0. The energy incident on the calorimeter is

$$E = 0.074\ E_0 . \qquad (4.10)$$

Of this energy, 18% is backscattered by the wire in the calorimeter (Baker, 1963); so

$$E = 0.061\ E_0 . \qquad (4.11)$$

By comparison with Equation (4.9), the relation reduces to

$$E_0' = 157.5\ (R - R_0)\ joules/\Omega . \qquad (4.12)$$

The resistance change is measured by means of the bridge circuit in Figure 4.2. Calibration is accomplished by switching a known resistance into the active arm of the bridge and by observing the galvanometer deflection. The microammeter in the circuit serves as a

means of determining the coarse balance of the bridge, before the galvanometer is introduced into the circuit.

On the most sensitive scale, the galvanometer deflection is typically 50 mm/0.1Ω. A deflection of 1 mm is easily detected; hence, the sensitivity is approximately

$$S = 1 \text{ mm}/0.002\Omega, \tag{4.13}$$

or in terms of total beam energy, E_0,

$$S = 1 \text{ mm}/0.3 \text{ joules}. \tag{4.14}$$

The relative intensity is obtained as a function of time by means of the phototube. With a knowledge of I(t) and the total energy, E,

$$I(t) = I_0 f(t), \tag{4.15}$$

The energy may be expressed

$$E = I_0 \int_0^\infty f(t)\, dt \tag{4.16}$$

or

$$I_0 = \frac{E}{\int_0^\infty f(t)\, dt}.$$

The power output is given by the relation,

$$P(t) = \frac{E\, f(t)}{\int_0^\infty f(t)\, dt}. \tag{4.17}$$

Vacuum Ultraviolet Spectrograph

A vacuum ultraviolet spectrograph was constructed for the laboratory (Payne and Todd, 1966) and is in the process of being calibrated. It will be employed to obtain spectrographic information about the plasma which is produced by the incidence of the laser beam on the target. This spectrograph employs the Rowland circle mounting and is

operated at near grazing incidence. The spectrograph will be attached to the target enclosure by removing the window, and using an adapting flange.

The spectrograph is presently capable of resolving lines between about 100 and 1400 A. By analyzing the spectra of the flash from the exploding plasma, the various ionic species in the plasma may, in principle be determined. The spectra is to be obtained in conjunction with the measurements that are discussed in the previous section. The laser output measurement is a permanent part of the assembled equipment, and measurements are to be obtained during each run.

In addition to the spectrographic analysis, several time exposure photographs of the plasma will be obtained. A Voightlander, 35 mm camera for color film is mounted outside the target enclosure at the viewing port and is focused on the point of incidence of the laser beam.

Quadrupole Mass Filter

In order to determine relative ionic densities in the plasma from the laser beam incidence, a quadrupole mass filter is planned. It is an adaptation of a design that is described in current literature (Brubaker and Tull, 1964; Paul and Raether, 1955; Woodward and Crawford, 1963). As with all mass spectrographs, it may be employed to determine the relative concentration of various ionic species which have approximately the same mass. This data will be helpful in determining the physical properties of the plasma under study. In addition, information about the velocity distribution of each ionic species may be obtained by analysis of the data. In this section, the principles of

operation are developed for a quadrupole mass filter which may be employed for plasma analysis.

The quadrupole mass filter employs electric fields which permit only those ions which have a given ration of q/m to pass through it, while the others are rejected by the filter. This is accomplished by means of four cylindrical electrodes which are arranged and are connected as indicated in Figure 4.3.

As a consequence of the relation of r_0 to the rod diameter, $D = 2.30\ r_0$, there is a close approximation to the hyperbolic fields which are shown in Figure 4.4. Laplaces' equation is

$$\nabla^2 V = 0, \tag{4.18}$$

or

$$\frac{\partial^2 V}{\partial x^2} + \frac{\partial^2 V}{\partial y^2} + \frac{\partial^2 V}{\partial z^2} = 0 \tag{4.19}$$

Since opposite rods are similarily charged, a solution of the form,

$$V = \phi(t)\ (\alpha x^2 + \beta y^2 - \gamma z^2), \tag{4.20}$$

is assumed. For the surface,

$$\frac{y^2}{r_0^2} - \frac{z^2}{r_0^2} = 1 \tag{4.21}$$

the solution in Equation (4.20) must be

$$V = \phi(t). \tag{4.22}$$

For the surface,

$$-\frac{y^2}{r_0^2} + \frac{z^2}{r_0^2} = 1, \tag{4.23}$$

The solution in Equation (4.20) must be,

$$V = -\phi(t). \tag{4.24}$$

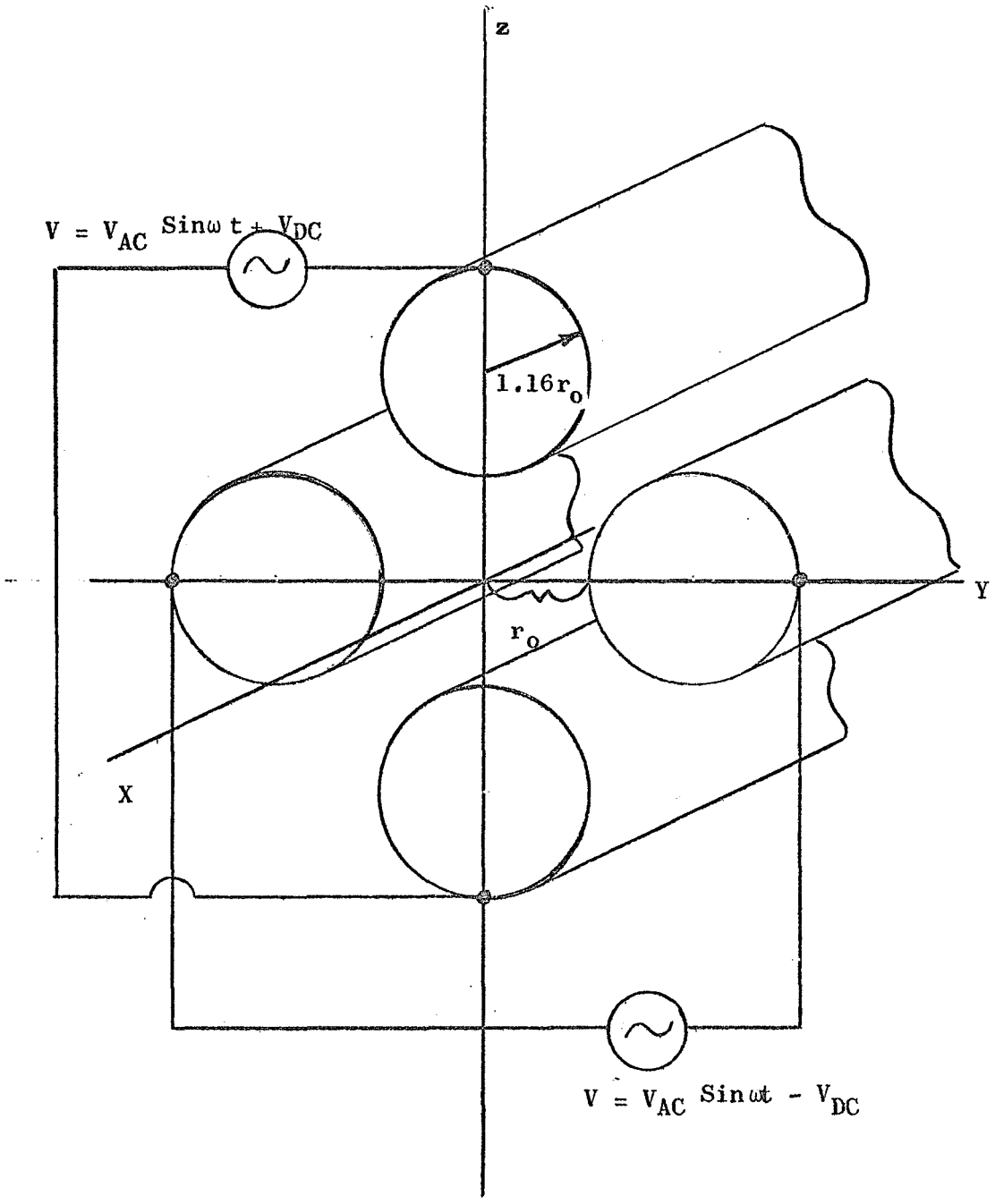

Figure 4.3. Quadrupole Mass Spectrometer Geometry.

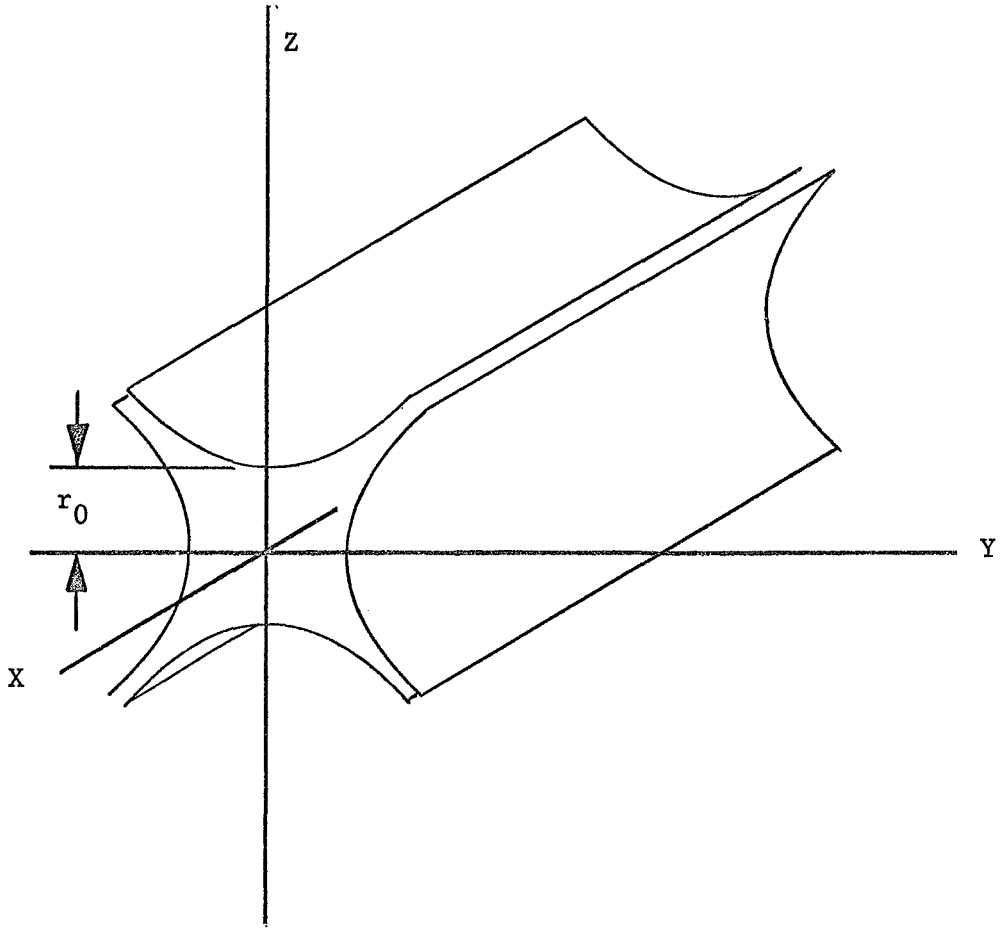

Figure 4.4. Hyperbolic Electrodes for Solving the Fields of the Quadrupole.

Substituting (4.20) into Laplaces' equation, a relation between the constants is obtained,

$$\alpha + \beta - \gamma = 0 \tag{4.25}$$

At the rod surfaces, the tangential field satisfies

$$\left(\frac{\partial V}{\partial x}\right)_{\text{surface}} = 0 \tag{4.26}$$

so

$$\phi(t)\ (2\alpha x) = 0 \tag{4.27}$$

or,

$$\alpha = 0. \tag{4.28}$$

By inserting the value of α into Equation (4.20),

$$V = \phi(t)\ (\beta y^2 - \gamma z^2). \tag{4.29}$$

By applying Equations (4.21) and (4.23), the value of β and γ are found,

$$\beta = \gamma = \frac{1}{r_0^2}. \tag{4.30}$$

The potential gradient is

$$\bar{E} = -\nabla V = \frac{2\phi(t)}{r_0^2}\ (-y\bar{j} + \bar{z}\bar{k}) \tag{4.31}$$

where j and k are unit vectors. The force on an ion of charge, Ze, is

$$F = ZeE \tag{4.32}$$

where e is the electronic charge and Z is the charge multiplicity of the ion. The equations of motion become

$$F = ma = m\left(\frac{d^2y}{dt^2}\,\bar{j} + \frac{d^2z}{dt^2}\,\bar{k}\right) \tag{4.33}$$

in which the components are

$$m\frac{d^2y}{dt^2} = -2Ze\,\frac{\phi(t)}{r_0^2}\,y \tag{4.34}$$

$$m \frac{d^2z}{dt^2} = + 2Ze \frac{\phi(t)}{r_0^2} z.$$

If the time variation of the field is

$$\phi(t) = V_{dc} + V_{ac} \cos \omega t, \tag{4.35}$$

the first part of Equation (4.34) becomes

$$m\ddot{y} = \frac{-2Zey}{r_0^2} (V_{DC} + V_{AC} \cos\omega t) \tag{4.36}$$

and the second part of this equation becomes

$$m\ddot{z} = \frac{+2Zez}{r_0^2} (V_{DC} + V_{AC} \cos\omega t). \tag{4.37}$$

If the field length is given by ℓ, the number of cycles an ion experiences in the filter is,

$$n = \frac{\ell\omega}{2\pi v_x} \tag{4.38}$$

Equations (4.36) and (4.37) are special cases of Mathieu's equation which may be stated in general form

$$\frac{d^2X}{d\zeta^2} + (a - 2q \cos 2\zeta) X = 0 \tag{4.39}$$

If Equations (4.36) and (4.37) are converted to this form, the constants may be evaluated

$$\zeta = \frac{\omega t}{2}, \quad a_y = \frac{+8ZeV_{DC}}{mr_0^2\omega^2}, \quad q_Y = \frac{-4ZeV_{AC}}{mr_0^2\omega^2}, \tag{4.40}$$

and

$$a_z = \frac{-8ZeV_{DC}}{mr_0^2\omega^2}, \quad q_z = \frac{+4ZeV_{AC}}{mr_0^2\omega^2} \tag{4.41}$$

The general solution of Equation (4.39) may be written as

$$X = A e^{\mu\zeta} \sum_{n=-\infty}^{\infty} C_n e^{in\zeta} + B e^{-\mu\zeta} \sum_{n=-\infty}^{\infty} C_n e^{-in\zeta}, \qquad (4.42)$$

which is stable provided the constant μ which depends on a and q, is a pure imaginary, otherwise the solution is unstable. In terms of trajectories, the unstable trajectory increases exponentially in amplitude, whereas the stable trajectory either decreases or remains constant. The ranges of stability are shown as a function of a and q in Figure 4.5.

From the graph, the stable ranges are symmetrical about q = 0. Since q is positive for z and negative for y, and is of the same magnitude for both, the path will be stable in both the y and z directions, provided the path is stable in q. As a consequence, only the absolute value of q is significant in determining stability. Since both a_y and a_z must satisfy stability requirements, the graph may be folded about a = 0 and only the absolute value considered. If the fold is made, the largest region of stability is shown in Figure 4.6. This graph presents the design criteria to determine the frequency, the field length, and the rod separation that are necessary to use the mass filter as an ion separator.

In order to determine the desired operating point and characteristics of the quadrupole mass filter, the physical measurement is examined. The plasma from the target will be composed of singly and multiply charged ions of the target material. Since the target material is aluminum, the mass of the ions will be,

$$M_{AL} = 27 \text{ amu} \qquad (4.43)$$

Assume maximum ionic velocity to be

$$v_{max} = 10^7 \text{ cm/sec} \qquad (4.44)$$

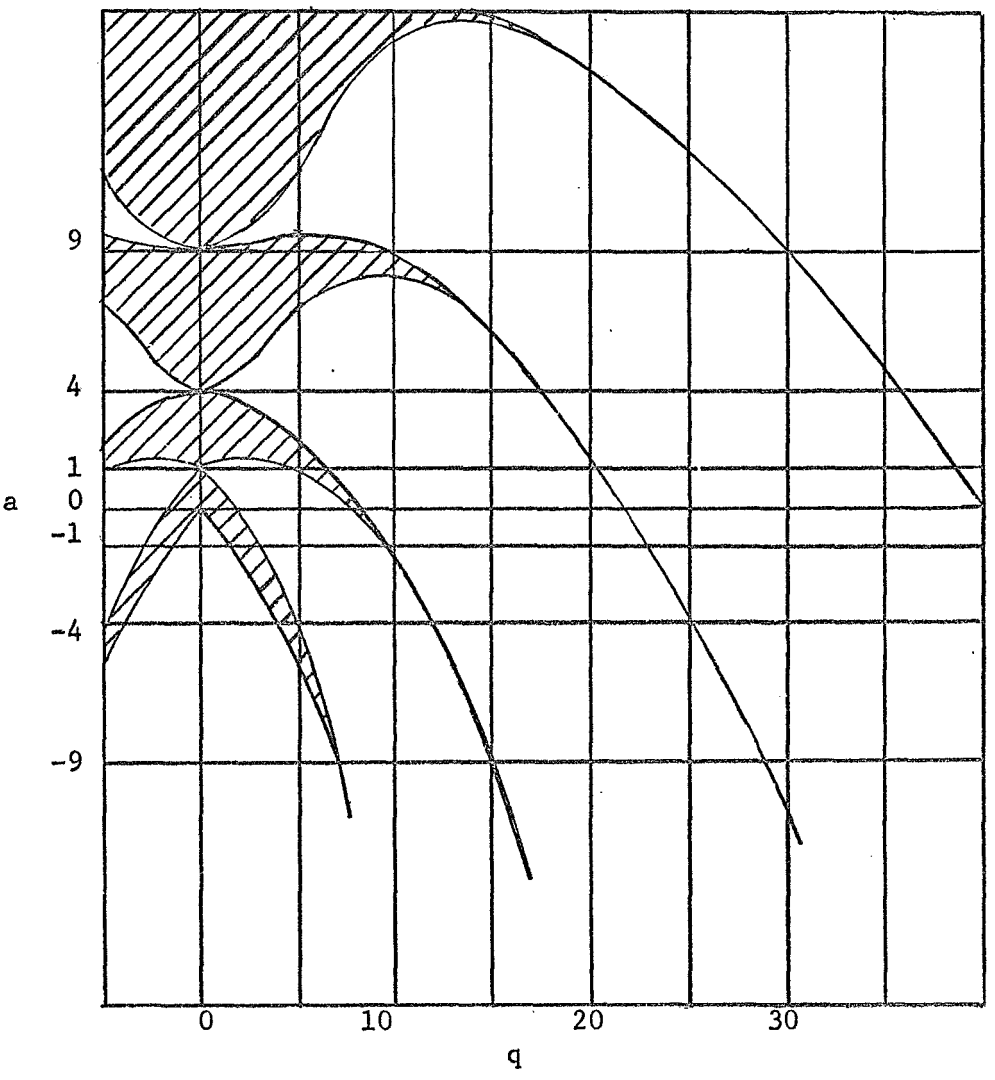

Figure 4.5. Ranges of Stability for Solutions of Mathieu Equation.

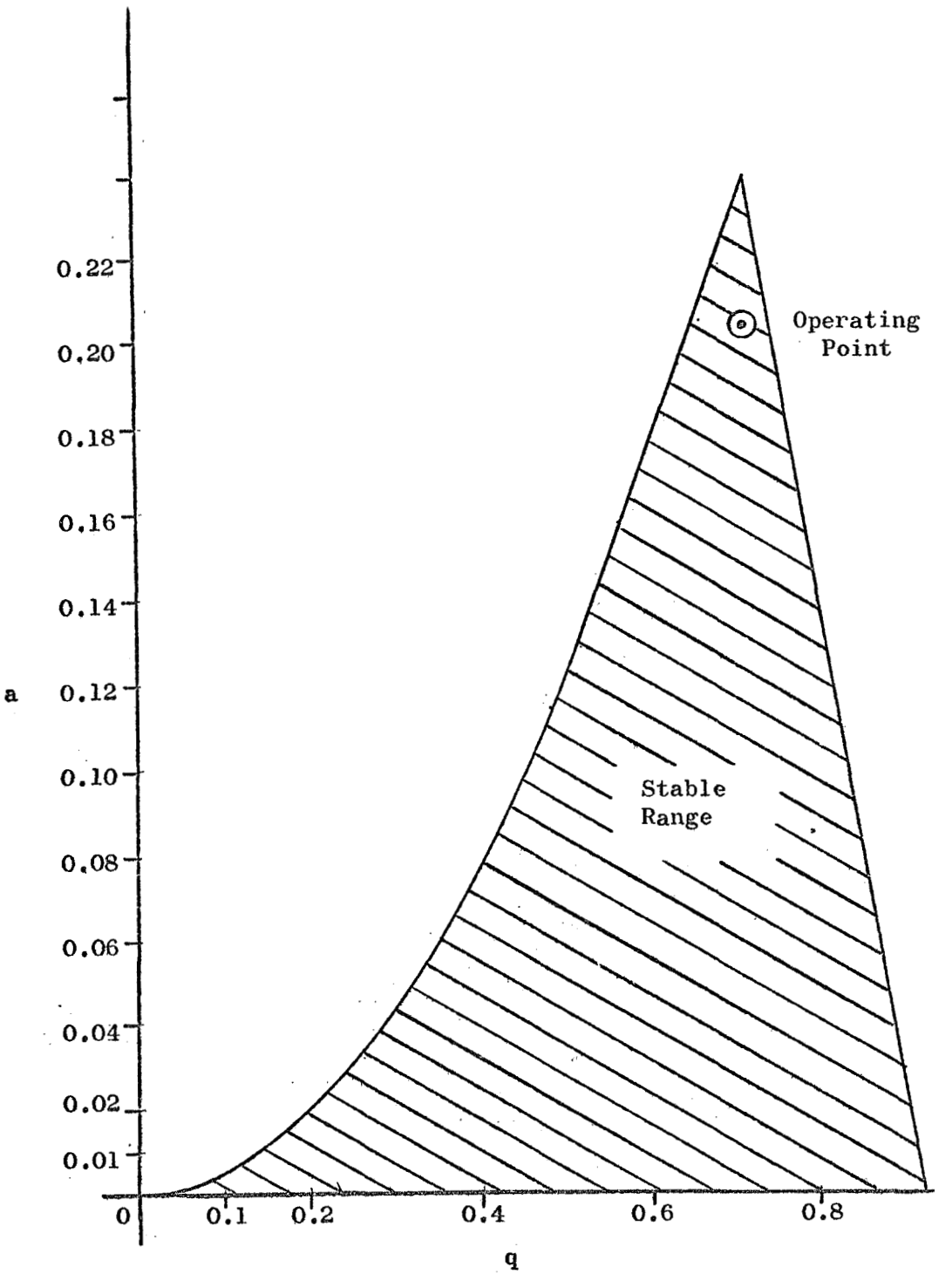

Figure 4.6. First Stability Range.

which corresponds to an energy of 10^4 Kev. From Equation (4.38), it is found that

$$N_{min} = \frac{\ell\omega}{2\pi v_{max}} , \tag{4.45}$$

or

$$N_{min} = \frac{\ell\omega}{2\pi} 10^{-7} . \tag{4.46}$$

For a practical design, assume a field length of 30 cm. and a frequency of 3.2 mc.,

$$N_{min} = 9.2 \text{ cycles.} \tag{4.47}$$

This is believed to be sufficient for ion separation, because charge on the ions changes in large steps. The measurements are made by maintaining a constant frequency and adjusting the parameters V_{ac} and V_{dc} to select a given ionic species. By reference to Figure 4.6, a good operating point would be

$$a = 0.20, \quad q = 0.70 \tag{4.48}$$

This point provides good resolution, and requires voltages which are easily attained. A convenient rod diameter of 13.23 mm was chosen, which requires

$$r_0 = 5.75 \text{ mm} \tag{4.49}$$

in order to obtain hyperbolic fields.

To ascertain the voltages that are necessary to transmit a given ionic species and to verify that the others are rejected, the values of a and q are obtained from Equations (4.40) and (4.48),

$$a = .20 = 2.14 \times 10^{-3} Z V_{DC} \tag{4.50}$$

and

$$q = .70 = 1.04 \times 10^{-3} Z V_{AC} \tag{4.51}$$

The voltages for each case are given by,

$$V_{AC} = \frac{655.4}{Z} \text{ volts}, \quad V_{DC} = \frac{93.63}{Z} \text{ volts}. \tag{4.52}$$

Five cases are considered separately.

Case I: Filter is set for the singly ionized ion where Z = 1.

Solving for the voltages

V_{ac} = 655.4 volts, V_{dc} = 93.63 volts

With these values of the voltages, the a and q values for the four higher species are:

Species	a	q
II	0.40	1.40
III	0.60	2.10
IV	0.80	2.80
V	1.00	3.50

By reference to Figure 4.6, all except the singly ionized species have unstable trajectories, and these ions will be rejected by the filter.

Case II: The filter is set to accept the second species, for which

V_{ac} = 327.7 volts and V_{dc} = 46.82 volts.

The a and q values for the other species are examined to verify that their trajectories are unstable.

Species	a	q
I	0.10	0.35
III	0.30	1.05
IV	0.40	1.40
V	0.50	1.75

Again, by referring to Figure 4.6, the trajectories are unstable for all except the second species.

Case III: The filter is set for ionic species III, triply ionized for which

V_{ac} = 218.5 volts and V_{dc} = 31.21 volts.

For the other species, the values of a and q are:

Species	a	q
I	0.067	0.23
II	0.134	0.46
IV	0.268	0.92
V	0.335	1.15

By reference to Figure 4.6, these trajectories are unstable, and the ions will be rejected.

Case IV: The filter is set for the fourth species, for which

V_{ac} = 163.85 volts and V_{dc} = 23.41 volts.

The parameters for the other species are:

Species	a	q
I	0.05	0.175
II	0.10	0.350
III	0.15	0.525
V	0.25	0.875

Again, the other species are rejected by the mass filter.

Case V: The filter is set for the fifth species, and the values are:

V_{ac} = 131.1 volts and V_{dc} = 18.73 volts.

For the other species, the parameters are:

Species	a	q
I	0.04	0.14
II	0.08	0.28
III	0.12	0.42
IV	0.16	0.56

These values lead to unstable trajectories, and the ions are rejected.

An examination of the preceding cases reveals that the species nearest to the accepted ion in charge are less strongly rejected than the other ions. The strength of this rejection also decreases as the charge number increases. As a consequence, if the filter is set for an ion with $Z \geq 8$, both the Z and the Z-1 ions are accepted. Measurements are not anticipated for ions having $Z \geq 5$. If measurements are required for ions with $Z \geq 5$, the operation point may be shifted toward the peak of Figure 4.6, and the filter will only accept the desired ion.

The requirements for ion filtering are summarized:

1. A field length of 30 cm. which requires four poles of diameter 13.23 mm and separation 11.50 mm.
2. A radio frequency generator which operates at 3.2 mc. and at an output range of from 0 to 1,000 volts peak to peak.
3. A dc power supply which is variable from 0 to 150 volts.

An rf power supply for a quadrupole mass filter is described in the literature (Woodward and Crawford, 1963). The dc voltages are obtained by rectifying a portion of the rf voltage. This insures a constant value of a/q in the event of a frequency drift or of a shift in the rf voltage.

At the present time, the circuits are being reviewed and the construction is to start shortly. The quadrupole mass filter will be mounted within the target enclosure, as near as possible, to the point of impact. Since the plasma is generated, almost instantaneously, the output of the mass filter as a function of time reflects the velocity distribution of the ion which the filter is set to accept. Provisions are made for several mounting positions and angles in order to determine the degree of spatial symmetry in the plasma during its expansion. At the present time, the mechanical design of the mass filter is in the planning stage.

CHAPTER V

RESULTS OF INITIAL TESTS

The primary intent of the research which is described in this thesis was the design and construction of a twin ruby laser assembly. In addition, some instrumentation was constructed for plasma studies. The experimental study itself, using this equipment, was not within the scope of this thesis. Some initial tests were necessary to determine the operating characteristics and to evaluate the performance of the assembly. The purpose of this chapter is to give a qualitative description of these initial tests and to offer some suggestions for improvement of the equipment.

General Description

The first tests with the laser system were to ascertain the triggering characteristics of the flashtubes. These tests were made prior to the installation of the inductors in the flashtube circuits. In addition, a single trigger transformer (Kemlite 4CM, 50:1) was employed to trigger both flashtubes. The primary of the trigger transformer was pulsed with a 200 volt pulse, so the trigger output pulse was about 10 KV. With this arrangement, the triggering was very erratic. At times, the flashtubes fired spontaneously. During these tests, two flashtubes were shattered as a consequence of the rapid current rise within the tubes.

Correspondence with Kemlite Corporation revealed that a ballast inductor should be used in each flashtube circuit in order to shape the discharge pulse. As a result of this correspondence, the primary trigger pulse was increased to 400 volts. Two transformers, connected in parallel as described in Chapter III, were employed. With this arrangement, approximately a 20 KV pulse is delivered to the trigger wire.

After these changes, another series of tests were conducted. These tests employed a capacitor storage at a voltage of approximately 7 KV. The rated voltage is 10 KV. The triggering was more reliable but the problem of spontaneous ignition remained. The laser was operated in the conventional mode and measurements of the laser output were attempted. Several energy readings were obtained with the calorimeter, and these were found to range up to 11 joules. Difficulty was experienced in obtaining a good phototube trace of the laser output. This difficulty was attributable, in part, to transients from the discharge of the energy storage capacitor. It was also difficult to gauge the magnitude of the phototube output in order to preset the oscilloscope. Much of this difficulty probably arose from capacity coupling to ground of the flashtube.

In addition to the calorimeter readings, various degrees of target deformation from the laser pulse were observed. This point is discussed, further, in the next section. Two time exposure photographs of the target were also obtained during this series of tests. The most striking one was obtained in the test where the laser beam energy was measured to be 11 joules. The time exposure shows an intense white flash, which is indicative of a plasma, at the region of impact. The background is illuminated by the scattered red light of the laser pulse.

Since these initial tests, some additional tests were attempted to obtain a phototube trace of the q-switched output. These tests have met with little success because of triggering difficulties. This problem will be discussed further in the final section of this chapter.

Target Deformation

Although these initial tests were not expressly for the purpose of studying laser beam impact, some types of target deformation were observed.

The laser pulse was focused to a spot of approximately 1 mm^2 on the target. Several types of targets were employed during these initial tests. Appreciable target deformation, however, was only observed on aluminum foil (0.001 in. thickness) and aluminum disks (0.030 in. thickness).

The incidence of the conventional laser pulse on the foil target melted a hole through the foil. The hole was in the shape of a diamond and had an area of approximately 1.25 mm^2. The hole was ringed with a ridge of metal which appeared to have melted and then resolidified. Unfortunately, a measurement of the laser pulse energy was not obtained for this particular firing, however, it was estimated to be about two joules.

The deformation at the zone of impact was observed for an aluminum disk. The most striking of these deformations was produced by a conventional laser pulse for which an energy of 11 joules was measured. The deformation, in this case, was crater shaped. Again, the crater was ringed with a ridge of resolidified metal. In addition, pits, much smaller than the crater itself were observed at the bottom of the crater.

The crater had roughly the same area as that of the focused laser pulse and a depth of from 0.001 to 0.002 inches.

Suggestions for Future Improvements

As in every undertaking of the type described in this thesis, there are a number of possible improvements. The purpose of this section is to indicate some of these and to offer suggestions for their improvement.

The foremost need is for a more reliable means of triggering the laser. At the present time, the triggering is erratic, and the problem of spontaneous ignition persists. At the time that two trigger transformers were installed in parallel, as is described in Chapter III, the primary trigger voltage was increased to 400 volts. This exceeds the voltage rating of the 4CM transformer. In spite of this, the laser has been successfully fired using the 4CM transformers. The most immediate answer to the triggering problem would be to change over to trigger transformers which have a higher voltage rating, such as Kemlite's model 5CM. The parallel connection of the pulse transformers has an inherent disadvantage. The impedance of the primary of each transformer depends on the impedance of the secondary. If the trigger wire, which is connected to the secondary, ionizes the flashtube, most of the trigger pulse will appear across this transformer. Because of this, the other flashtube will fail to respond to the trigger pulse. This difficulty could be removed by using two separate coincident trigger circuits, one for each flashtube. If the flashtubes could be operated at their rated voltage, special circuits for the transformers would not be necessary.

Another area, which could be improved, is the means of charging the energy storage banks. At the present time, a charging time of about 30 minutes is required to charge the bank to 7 KV. The reason for this is that the power supply, which was available in the laboratory, is limited to an output current of 20 milliamperes. Since the power supply has a maximum voltage output of 10 KV, the energy storage banks and the flashtubes had to be placed in a series parallel arrangement. The disadvantage of lengthy charging times is two-fold. The most obvious is the time required to ready the laser for a test. The other is that the capacitors are charged for an unnecessarily long time.

These problems could be resolved by acquiring a 20 KV power supply which has a higher current rating; then it would be possible to connect the capacitor banks and the flashtubes in series. This would insure that both tubes fire even if only one responds to the trigger pulse. In addition, a larger power supply would reduce the time that is required for the laser shot.

In line with this discussion, one of the problems is encountered in attempts to obtain a trace of the laser pulse, light intensity with a phototube. Electrical transients in the system triggered the oscilloscope prematurely, and no phototube trace was observed. These transients may also be responsible for the spontaneous ignition of the flashtubes. This situation can probably be remedied by a careful review of the grounding connections in the discharge circuit and in other circuits.

There are other aspects of the laser facility, which, in the course of time, will probably be improved. It is felt, however, that if some of the improvements which have been mentioned in this section are

included, the laser facility may be employed effectively for the study of laser-produced plasmas.

SELECTED BIBLIOGRAPHY

Gregg, D. W., and S. J. Thomas. 1966. Kinetic Energies of Ions Produced by Laser Giant Pulses. Jour. App. Phys., Vol. 37; 4313-4316.

Vogel, K., and P. Backund. 1965. Application of Electron and Optical Microscopy in Studying Laser Irradiated Metal Surfaces. J. App. Phys., Vol. 36; 3693-4054.

Lengyel, B. A. 1966. Introduction to Laser Phsyics. Wiley and Sons.

Bowness, C. 1965. On the Efficiency of Single and Multiple Elliptical Cavities. App. Opt., Vol. 4; 103-107.

Kaflas, P., J. I. Masters, and E. M. E. Murray. 1964. Photosensitive Liquid Used as a Nondestructive Passive Q-Switch in a Ruby Laser. J. App. Phys., Vol. 35; 2349-2350.

Baker, R. M. 1963. Measuring Laser Output with a Rat's Nest Calorimeter. Electronics, February 1, 36-38.

Payne, R. D., and F. C. Todd. 1966. A Spectrograph for the Far-Ultraviolet. Proc. Okla. Acad. Sci., Vol. 46; 115-121.

Brubaker, W. M., and J. Tuul. 1964. Performance Studies of a Quadrupole Mass Filter. Rev. Sci. Inst., Vol. 35; 1007-1010.

Paul, W., and M. Raether. 1955. Das Electrishce Massenfilter. Zeit. fur Phys., Vol. 140; 262-273.

Woodward, C. E., and C. K. Crawford. 1963. Design of a Quadruople Mass Spectrometer. Lab. for Insulation Res., Mass. Inst. of Tech., Tech. Rep. 176, NP-12543.